ABSTRACT

GPU SIMULATIONS IN MULTIPHASIC NANOSOLIDS AND SUPERCONDUCTING NANOSTRUCTURES

Ivan Viti, Ph.D.
Department of Physics
Northern Illinois University, 2016
Andreas Glatz, Director

With the ever-increasing availability of computing power, namely from Graphics Processing Units (GPUs), comes the responsibility to simulate more complicated systems. Complex functions such as the Ginzburg-Landau function can not be studied analytically for mesoscopic phenomena. Similarly, a thorough understanding of variable range hopping in electrons requires a Markov-Chain Monte-Carlo algorithm. With this in mind we computationally study two cases of condensed matter physics, thermoelectrics and superconductor-bound vortices. Here, We develop and implement a novel algorithm for simulation of variable-range-hopping of electrons in a nanosolid. We exploit the similarities between granule hopping and electrons in a coulomb glass. We also created an ad-hoc cluster in order to run these and other simulations. We benchmark this code using well studied Coulomb Glass theories, then make predictions on what Seebeck coefficients will be in various conductor-semiconductor combinations. Vortex-vortex interactions and vortex-inclusion interactions are not very well understood analytically. The mathematics becomes near-impossible when taken to mesoscopic scales. Applied temperature, magnetic field, or currents only serve to complicate the system. Yet these are all factors that need to be well understood before serious applications

can take place. Here we report two basic systems, The effect of vortex-inclusion matching on the effective resistance, and a novel funnel system for slowing the vortices. We describe how matching the number of inclusions to the number of vortices can help reduce the amount of vortex-induced resistance. We also describe how an aperture-type system can help to slow down vortices as they are travelling through the system draining energy.

NORTHERN ILLINOIS UNIVERSITY
DE KALB, ILLINOIS

OCTOBER 2016

GPU SIMULATIONS IN MULTIPHASIC NANOSOLIDS AND SUPERCONDUCTING NANOSTRUCTURES

BY

IVAN VITI

A DISSERTATION SUBMITTED TO THE GRADUATE SCHOOL
IN PARTIAL FULFILLMENT OF THE REQUIREMENTS
FOR THE DEGREE
DOCTOR OF PHILOSOPHY

DEPARTMENT OF PHYSICS

Dissertation Director:
Andreas Glatz

ACKNOWLEDGEMENTS

I would like to thank Andreas Glatz for his constant guidance. I would also like to thank the computer science department for allowing us to use their Gaea cluster for our simulations, as well as the Physics department for housing our Thoon cluster. Ivan Sadovsky was incredibly helpful in getting started with GL.

This work is supported by a grant from the DoE. The Rhoten-Smith fellowship and the Great Journeys fellowship also provided much needed funding.

TABLE OF CONTENTS

Chapter Page

LIST OF FIGURES

Figure Page

Figure Page

CHAPTER 1

INTRODUCTION

1.1 Geometric Pinning in Superconductors

As most materials are cooled, their resistance decreases. At these temperatures, electrons can no longer be considered particles bouncing around from ion to ion. Instead, if the material conditions are right, they form Cooper pairs and begin to propagate losslessly throughout the system. Phenomenologically they must be thought of as a wave-function [25]. Currents in an ideal superconductor, once set up, will continue to propagate indefinitely. Setting up a current in a superconductor is as simple as placing a magnet near one. The magnet will cause electrons to propagate in said magnet such that the external magnetic field is cancelled out. This kicking out of magnetic fields from superconductors is called the Meissner effect and is the second fundamental property of a superconductor.

A superconductor is different than a perfect conductor however. Following Maxwell's laws one would expect a perfect conductor to absorb and keep any magnetic field that one places near it. This is not the case for superconductors. They will try to kick out any magnetic field that is placed nearby. This is also the starting point to differentiate type 1 superconductors from type 2. Type 1 superconductors have a saturation magnetic field. After the magnetic field reaches a certain point, the superconducive properties of the material are removed. In type 2 superconductors, Vortices push their way into the superconductor in sufficiently high magnetic fields and can be seen as single quanta of magnetic flux made up of supercurrents circulating around normal cores [47]. The reason being that the wavefunction

which governs the field must be continuous and so the phase must go through a factor of 2π in order to line up with itself around the core. In the core, the superconductive order parameter is suppressed. Superconductors are valuable for an ever-expanding range of uses. Some prominent examples are magnets, qubits, voltage to frequency converters. It would be greatly beneficial if energy could be transfered losslessly across large distances. Theoretically this should be possible with superconductors. Practically we come across the problematic phenomena known as dissipation. In this dissertation we study this effect on the induced voltage in the system. A "hand-waving" approach to this helps us understand why vortices are important. They can be seen as a magnetic flux in the direction of the field. If a current is then applied perpendicular to this field, the vortices will move in a direction perpendicular to these two vectors. This movement will due to the Lorentz force, which will drain energy from the system. This drain is then measured from the voltage gap which appears in the material. Dr. Glatz wrote a program called GLGPU which models the important parameter function ψ using the time dependent Ginzburg Landau equations:

$$\Gamma(\partial_t + i\frac{2e}{\hbar}\mu)\psi = a_0\epsilon(r)\psi - b|\psi|^2\psi + \frac{1}{4m}(\hbar\Delta + \frac{2e}{ic}A)^2\psi + \xi(r,t) \tag{1.1}$$

and

$$\kappa^2\nabla \times (\nabla \times A) = J_n + J_s + I, \tag{1.2}$$

where $u = \Gamma/(a_0 t_0)$, t_0 is the unit of time, and J is the total current density. This program models a discretized system which is initialized with a parameter function and then each timestep is defined by following the TDGL equation. Using this program, we studied many situations such as grids of non-superconducting inclusions, funnels, vortex ratchets, and critical currents.

1.2 Dynamics In Artificial Solids

In 1755, the first thermodynamic refrigerator was created by William Cullen. He used a pump to lower the pressure over diethyl ether, which caused it to evaporate and absorb heat [23]. He learned that using phase differences were one way to transport heat. A liquid sticks together because these particles are attracted to each other and have "fallen together" into a lower energy state. It then makes sense that in order to break these particles apart (boiling), energy must be supplied. In Cullen's experiment this energy came from the thermal energy of the surroundings, thereby cooling the system. One can also see this from the point of view of entropy. Entropy is a quantification of the randomness of a system. In other words, how many possible states a system could have been in. Entropy can only stay the same or increase. In this case, when the liquid expanded to a gas, the number of possible states of the system dramatically increased as there was more volume for the molecules to occupy. This then led to a cooling of the system. Mathematically, entropy has two definitions. The first relates heat energy being exchanged at different temperatures. That is, the entropy of the system can be changed by moving around the same amount of heat at different temperatures. The second relates the number of possible states to the entropy of the system via Boltzmann's constant. In other words, as the number of possible states goes up, so does the entropy. Since then, engineers have found better, more efficient ways of creating temperature differentials. Better liquids which had more sought after phase characteristics such as freon were discovered. The system was also transformed into a cycle which could be used to pump heat out of the inside of the refrigerator and pump it to the outside. Any material that has the ability to change it's entropy can be used to create a thermal gradient. One of the more exotic -yet simple- examples is the rubber band refrigerator. When a rubber band is stretched quickly, it increases in temperature. This is because rubber bands

are long chains of randomly wound up polymers. When these polymers are pulled appart and stretched, the number of posible states decreases as they are forced into a straight line. The entropy has to go somewhere which ends up being the thermal noise (i.e. temperature) of the system. This heat should then be released into the environment. Once cooled to ambient temperature, the rubber band can then be placed in whatever enclosure one is trying to cool. There, the rubber band can be allowed to contract again. The particles now seeing that they have a lot more possible states of entropy, cool down and absorb heat from the system. The process can then be started over again by taking the rubber band out of the enclosure and stretching it out [24]. This process is called a heat cycle and is the basis of all refrigerators. Even without a phase change, one can move heat around by changing the system's pressure. This can be in the form of a gas, as in the case of stirling engines, or in the form of electrons as in the case of Seebeck devices. In 1821 Thomas Seebeck discovered that when two metals of different temperatures were put together, a compass needle would be slightly deflected. This is because the heat caused electron energy levels to become shifter. This led to a current when the electrons were placed together, which caused a magnetic field which deflected the compass [46]. Thermoelectric devices can be used to turn thermal gradients into electricity (Seebeck effect). They can also be used to turn electric power into cooling or heating (Peltier effect). Most modern refrigeration techniques require compression of some fluid which by defintion means moving parts. They also involve some sort of fluid that can degrade, corrode, or escape. A Peltier device can do this much more simply. A qualitative explanation to how they work is as follows; Electrons in the device can be pushed towards one side using an electric field. That side will become hot due to the thermodynamic "pressure". Conversely, the side losing electrons becomes cold. This process is reversed in systems where the charge carrier is positive.

Once again, technology found better materials which could be used to cool the system better.The next generation of thermal gradient to electric current conversion will be based

on careful alteration of the thermoelectric properties of materials [22]. The point of the alterations is to create a material which is insulating enough to keep the temperature gradient from equilibrating, yet conductive enough to let electrons through. Novel nanosolid materials can achieve this feat and push the boundaries of their thermoelectric capability. Currently Peltier devices can only acheive 12% of maximum theoretical efficiency compared to compressor refrigerators which can acheive 60%. By constructing artificial nanosolids, we can manipulate which electrons can transfer heat, thereby dictating the thermal conductivity. Nanosolids also have the ability to scatter phonons, thereby further insulating the system [7]. By tuning the properties of these granules, the figure of merit can be increased. Precise tuning would take many iterations of experimentation. Our approach was to write a parallel Monte-Carlo simulator called DIAS (Dynamics In Artificial nanoSolids). With this, we model the electrons' variable range hopping properties. Because electrons conduct most of the heat, and all of the electricity, We can then know the system's thermoelectric properties. Thus by creating a thermal gradient and comparing it to an electric gradient, we find the system's figure of merit.

The nano-grain electron system is not entirely understood analytically. However, it shares enough of its properties with the more complete Coulomb glass model that it makes sense to study the Coulomb glass as well. The Coulomb glass is a microscopic system where electrons attempt to transport by tunneling, yet get in each other's way due to the Coulomb blockade.

1.3 Condensed Matter GPU simulations

We could spend years building them and experimentally testing artificial nanosolids, but with the underlying physics being well-understood it is easier to simulate them. We could even spend years running these simulations in series on a CPU. The parallel simulation of

physical systems is the central pillar of this dissertation. By using Nvidia's CUDA and GTX-570 video cards, we parallelize the code on GPUs which allow all cell probabilities to be measured at the same time with no cost to performance. This dissertation will focus on the two most promising systems;vortex jamming/pinning in superconductors, and electron hop studies in thermoelectrics. We begin by explaining some of the theory and background of the GPU simulation of the time dependent Ginzburg-Landau system. Then we show how jamming and inclusion-vortex commensurability increases the depinning current. Afterwards, we then go into some depth on Dias and how it works.

CHAPTER 2

GEOMETRIC VORTEX PINNING

2.1 London Superconductivity

Superconductivity was first explained throught he light of Maxwell's equations. In 1935, Fritz and Heinz London used their equations to explain the Meissner effect. these can be derived from Ampere's law:

$$\nabla \times \overrightarrow{B} = \mu_0 \overrightarrow{J}, \tag{2.1}$$

where $\overrightarrow{B}$ is the magnetic field, μ_0 is the permeability of free space, and $\overrightarrow{J}$ is the current. We then use the vector identity

$$\nabla \times \nabla \times \overrightarrow{A} = -\nabla^2 \overrightarrow{A}, \tag{2.2}$$

to get

$$\nabla^2 B = \frac{B}{\lambda_p^2}, \tag{2.3}$$

where λ_p is the penetration depth. While these equations were good at describing the macroscopic properties of superconductors, better theories such as the Langevin system had to be derived to describe vortices.

2.2 Langevin system for vortices

The Langevin system for vortices is a relatively simple place to start. It keeps only vortex degrees of freedom and foregoes all other perturbations of the complex order parameter. As long as the pinning centers are not too dense and vortices stay further appart than their coherence length, this provides a fairly accurate system. Looking at the equation of motion for this overdamped system, one can get an idea of the forces involved:

$$\eta \frac{\partial u}{\partial t} = \epsilon_1 \frac{\partial^2 u}{\partial z^2} + \Sigma_j F_{vp}(u - R)\delta(z - z_j) + j + F_T(z, t), \tag{2.4}$$

where η is the viscosity coefficient, ϵ is the line tension, f is the current's driving force, (R, Z) are the random pinning coordinates, F_{vp} is the pinning force, and F_T is the thermal randomizing force. From this equation, one can see that the current driving force is trying to push overdamped vortices through a viscous fluid. Every once in a while, they get stuck in pinning centers and may or may not get out again depending on the current force and the thermal noise. Finally if the system is in 3 dimensions, then the vortices will want to stay in as straight of a line as possible [47]. As simple and intuitive as the Langevin system may be, it falls short on explaining other important phenomena such as vortex creation, cutting, and reconnection. Also, it cannot explain phenomena related to T_C variation. For these we need a much more powerful system called the time dependent Ginzburg Landau model.

2.3 The Ginzburg-Landau Model for Superconductivity

Superconductivity near the transition temperature can be succinctly characterized by a complex order parameter field ψ. Near this critical temperature, the free energy of the system becomes

$$F = F_n + \alpha|\psi|^2 + \frac{\beta}{2}|\psi|^4 + \frac{1}{2m}|(-i\hbar\nabla - 2e\overrightarrow{A})\psi|^2 + \frac{|\overrightarrow{B}|^2}{2\mu_0} \tag{2.5}$$

where F_n is the free energy, α and β are system constants which will be defined later,μ_0 is the magnetic permeability of free space , m is the cooper pair effective mass, e is electron charge, $\overrightarrow{A}$ is the magnetic vector potential, and $\overrightarrow{B}$ is the magnetic field. Being interested in the physical reprecussions of this kind of system, we minimize the free energy with respect to the order parameter and vector potential to get

$$\alpha\psi + \beta|\psi|^2\psi + \frac{1}{2m}(-i\hbar\nabla - 2e\overrightarrow{A})^2\psi = 0 \tag{2.6}$$

$$\nabla \times \overrightarrow{B} = \mu_0 \overrightarrow{j} \tag{2.7}$$

$$\overrightarrow{j} = \frac{2e}{m} Re(\psi^*(-i\hbar\nabla - 2e\overrightarrow{A})\psi) \tag{2.8}$$

where j is the current and Re is the real part. Equation 2.6 can be thought of in two parts. The first part $(\alpha\psi + \beta|\psi|^2\psi)$ is just the component relating to the superconductor, without supercurrent. Above the superconducting temperature, only $\psi = 0$ solves the equation.

Below the superconducting temperature we have $|\psi|^2 = -\frac{\alpha}{beta}$, which is reminiscent of a quantum observable. The second half of 2.6 is basically a modified version of the Schrodinger time-independent equation, but with a magnetic potential. 2.7 is Ampere's law. 2.8 is also similar to a quantum observable with $-i\hbar\nabla - 2e\overrightarrow{A}$ as the momentum operator in the presence of a magnetic field. The Ginzburg-Landau equations can be related to the microscopic Bardeen-Cooper-Schrieffer theory [18].

2.4 Large λ Limit

The surface of a superconducting field is a rich interplay between the coherence length $\xi = \sqrt{\hbar^2/4ma_o}$ and the magnetic penetration length $\lambda = \sqrt{mc^2/8\pi e^2\psi_0^2}$, where $\psi = \sqrt{a_0/b_0}$ is the equilibrium value of the order parameter in the absence of an electromagnetic field. The ratio $\chi = \lambda/\xi$ is called the GL parameter.

In high temperature superconductors, the penetration length λ is typically much larger than the coherence length ξ. One consequence of this is that at length scales smaller than λ, the magnetic field is basically constant. The coherence length comes from the fermi velocity for the material and the energy gap between conducting and superconducting states [26]. ξ describes the length over which the superconducting electron density can change. This is also the size to which a cooper pair can spread. Another place it comes in is determining the size of the core of the vortex.

2.5 Phenomenological Vortex Interactions

2.5.1 Vortex-Vortex Interactions

Vortex flux lines will move due to Lorentz forces $W = d \cdot F = d \cdot (B \times I)$ where W is the energy drained away by moving vortices, d is the distance the vortex travels, F is the force on the vortex, B is the field of the vortex, and I is the current of the system. Whether or not a vortex will move is complicated and hard to study analytically. There are many factors which affect the movement of a vortex. First, vortices which rotate in the same direction will push each other away 2.1. Conversely, if the vortices spin in the same direction, they will attract and annihilate each other 2.2. This can be explained if one looks at the lorentz forces of a vortex-vortex system.

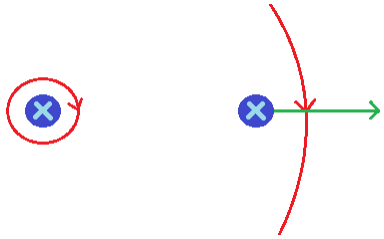

Figure 2.1: The right hand rule tells us which direction the currents will swirl around a vortex pointing into the page. Then using Lorentz's law at the second vortex, we can see that the second vortex will be pushed away. The same thing is happening from the current of the second vortex onto the first.

2.5.2 Vortex-Defect Interactions

The interaction between vortices and defects have been well-studied. Defects can be used to pin vortices and reduce dissipation. Defects can be impurities, vacancies, and inclusions.

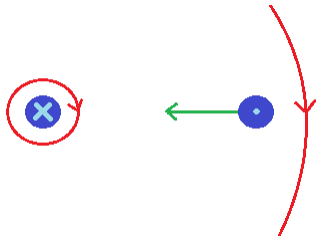

Figure 2.2: The right hand rule tells us which direction the currents will swirl around a vortex pointing into the page. Then using Lorentz's law at the second vortex, we can see that the second vortex will be pulled in this time. The same thing is happening from the current of the second vortex onto the first (although the second current flows in the opposite direction).

In one dimension they can be defects such as dislocations and irradiation tracks. Finally in three dimensions, they can be twin boundaries or stacking faults. The structure of atomic defects can have scattering properties which are either potential or magnetic type. Cooper pair-breaking caused by these defects has the effect of lowering the critical temperature. While studying these is important for pinning dynamics, it is the defecs which are on the order of several coherence lengths which are of interest to us. In three dimensions one can create columnar defects in the direction of the expected magnetic field. These have the strongest ability to hold on to vortices while causing the least amount of obstruction [47].

2.5.3 Vortex-Wall Interactions

The substrate is not always superconducting. It is also possible to embed non-superconducting components into the system. Since the super-current is suppressed in this system, There are many interesting effects to observe near these zones. First, a vortex near a magnetically neutral non-superconducting zone will be attracted to it. This can be seen as a type of "Venturi effect". Since the current flux must be conserved around a vortex, and there is not as much room for it to flow on the side closest to the wall, the current increases. A

difference in current flux on opposing sides of the vortex then creates a force in the direction of the wall. The vortex is then pulled into the wall. The vortex will tend to remain there until pushed out by an external force. Two of the most common forces are external applied current and other vortices.

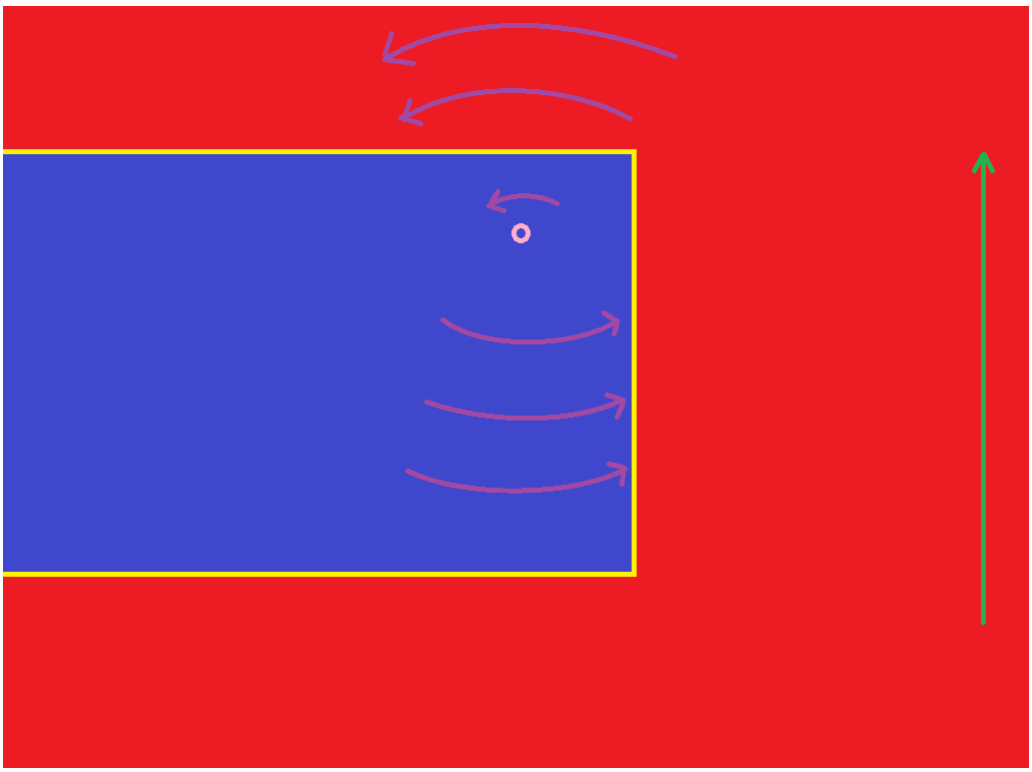

Figure 2.3: Vortices (pink) will tend to get stuck inside inclusions (blue). That is because the supercurrent will travel faster outside of the inclusion, diminishing the amount of supercurrent inside. The vortex will therefore feel a force away from the boundary with the stronger superconductor.

2.6 Relevant Vortex studies

Type 2 superconductors, while working at liquid nitrogen temperatures, have the problem of energy dissipation due to vortex dynamics. Therefore many geometric solutions are being

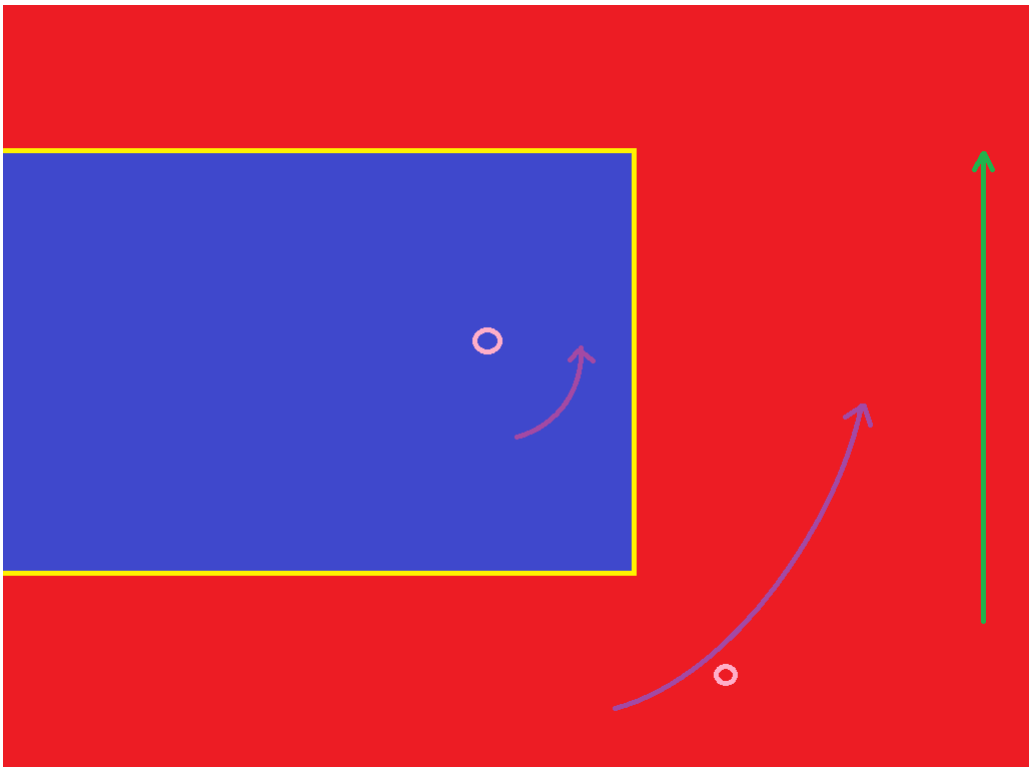

Figure 2.4: Once a vortex is stuck inside an inclusion, it will repel any other vortices which come near it.

worked on to try to slow down this energy loss. Here we focus on two of the most promising, vortex matching and funneling.

2.7 Vortex Matching and δT_c Pinning

With improvements in nanotechnology, it has become easier to create grids of inclusions. These can be made by inserting nanorods of different critical superconducting temperature (T_c), pulsed laser deposition , by using ion beams to disrupt the superconducting lattice, or by using lithographic techniques.

Inserting nanorods of materials using bulk targets has is benefits and problems. These nanorods can be made to have different T_c by controling the crystalinity or the amount of oxygen doping. [29] found a positive vortex-pinning effect due to the nanorods up to a magnetic field of 5 Tesla. They calculated the inter-vortex distance and designed a particular nanorod density. From there they were able to show that vortex-matching had a stronger pinning effect on the system. Varying the T_c of the system is a powerful way to control the vortex dynamics.

Pulsed laser deposition of YBCO can extend the irreversibility of magnetic fields past the 10 Tesla marker. This was done by using BYTO additions to pin the fluxes. All of this is thanks to the increased availability of ordered nanosized oxide secondary phases in epitaxial thin films. This allows the tuning of material functionalities and has various applications including high temperature superconductors. They observed a large improvement to the critical current compared to untouched YBCO [30]. Accurate placement of inclusions is important as inter-vortex forces are on the order of $1/r$.

Ion beam etching can also be used to create the necessary inclusions. These antidot arrays can be made on thin films of Niobium Nitride using reactive dc sputtering. The

antidot arrays are then created using a mask-aligner to do the ion-beam etching. They find experimental evidence for the observation that the maximum number of vortices which can be captured by an antidot of diameter d is

$$n_s = \frac{d}{4\xi(t)}, \tag{2.9}$$

where $\xi(t) = \xi_0/\sqrt{1-t}$ and t is a reduced temperature, typically in the range of $0.9 - 0.95$. They also found that vortices would become trapped in the antidots as well as in the interstices of the antidot lattice. This means that the critical current depends on the geometry of the lattice as well as the direction of current [31]. Multiple vortex antidots and inter-vortex trapping are important phenomenta when studying vortex matching. A theoretical basis for vortex matching has also been found. Berdiyorov et. al. [36] used the nonlinear Ginzburg-Landau theory to obtain all configurations for vortices in a grid of defects. They also find that vortices will pin in the inclusions and in between them. For small inclusions, they find only one vortex is trapped per hole. The hole radius and inter-hole distance determines the ability of multiple vortices to be forced into the holes. Like spheres in a box, The vortices prefer a triangular lattice as that affords the densest packing. If the pinning force of the holes becomes small enough, the lattices shift from the grid imposed quadratic lattice to a more natural triangular lattice. They find matching effects at whole and fractional magnatic field to hole ratios. Finally, they found their results to not agree with the Little-Parks theory of superconductors.

Lithographic (sputter etching) techniques were used to create arrays of submicrometere sized pinning arrays. These were compared to simulated J_c curves using the time dependent Ginzburg Landau model. They found that the critical current exibited maxima at the expected matching fields at 2.3 degrees Kelvin. The critical current was considerably larger than systems without antidot arrays [32]. It is important to have a physical temper-

ature at which these phenomena occur as most Ginzburg-Landau simulations only describe temperature in relation to T_c.

2.8 Vortex Jamming and Geometric Pinning

Another way to increase the depinning current of a system is to get the vortices to pin each other. This jamming effect can be accomplished by manipulating the geometry of the system they must past through. Different geometric strategies have been tried including simple funnels, diamonds, and conformal maps. Vortex ratchets and fluxon pumps are also of great interest in the superconducting world. These use diode-like geometries to keep vortices going in one direction. These effects can be seen even with a symmetric force such as an alternating current.

Computer simulations have been popular in demonstrating the usefulness of vortex ratchets. Within these ratchets, vortices will go through certain phases depending on the strength of the magnetic field. These phases are known as triangular, smectic, disordered, and square [33]. They showed that sawtooth ridges which modulate the z-component of a superconductor can have a similar effect as triangular modulations in the x and y-components. They used a Langevin model to simulate the vortices, which starts to become unphysical as the vortex density increases.

The optimal size of the funnel tip is such that only one vortex can pass at a time due to vortex-vortex repulsion forces. Reichhardt et. al. [27] , through the help of simulations, observed that the sum of the vortex velocities remains constant with increasing magnetic field. They highlight the similarities to a granular hopper, decreasing the width of the hopper aperture decreases the flow of grains. They found that as the number of vortices

increases, the pinned vortex structure becomes larger and harder to deform. This then keeps individuals from passing through the bottleneck.

Fluxon pumps can be used to extract useful work from a fluctuating environment. The vortex ratchet can be used as a fluxon rectifier. These could be used as fluxon lenses to concentrate or disperse magnetic fields. These would have various uses including dispersing trapped flux in SQUID magnetometers. But to get the desired effects, the frequency must hit the appropriate resonance region [34]. This means not only the right frequency for the geometry, but also the correct temperature (i.e. random motion). Thermal noise had to be kept low in the pinning systems. Like sand in an hourglass, minor turbulence has a large effect on the ability of vortices to stick. They again back up the idea that the more fluxons one has, the more their motion will be restricted.

Vortices travelling through constricting lattices can also be used to study the dynamics of interacting particles travelling through confining potentials. Yu et. al. found that with the correct geometry, vortices would begin moving as the external magnetic field varied [35]. They found strong matching effects between the vortex distribution and the constriction lattice. By tailoring their diamond shaped channel, they could pick their confining potential. The angle of the wall has a strong effect on the ability of the system to be immobilized.

We built upon previous GLGPU research in geometric pinning. In order to simulate geometrical constraints and voids of various shapes we impose appropriate internal boundary conditions or use unstructured grid discretizations [47]. The boundary conditions are imposed via picking no current (open) boundaries which simulate insulating inclusions [18]. Multiple types of tesselations are also possible, including checkerboard, or less standard Voronoi tesselations. These are useful for polycrystalline thin superconducting films with variations of T_c.

2.9 GLGPU overview

GLGPU is a GPU-based Jacobi solver for the time-dependent GL equations. It was designed to solve mesoscale problems which arised in superconductor design. Instead of treating the vortices as elastic strings in a viscous medium, it focuses on the underlying order parameter. This allows for correct interactions between pairs of vortices, vortices and inclusions, and allows the vortices to split up and rejoin. To model the system accurately, we need to take into account the Ginzburg Landau function at a microscopic resolution as a complex valued scalar field. The amplitude of this field is related to the supercondonductivity density, while the phase is related to the current of the system (after a gauge transformation). Through careful optimization, the system size can be made large enough to encompass many vortex interactions and complicated non-superconducting architectures. Physical pinning defects are simulated as modulations of the superconductor's critical temperature. The simulation works by first integrating the GL equations forward in time, then solving the Poisson equiation to find the electric and magnetic fields. There are also noise correlation terms to simulate thermal effects [18].

2.9.1 stable GLGPU system

The particular Ginzburg Landau equations which were used are designed to be particularly stable. In appendix 1, we explore the limits of this system and find it works for all relevant currents. These current equations were :

$$J_N = -\sigma[(1/c)\partial_t A + \nabla\mu] \tag{2.10}$$

and

$$J_S = -\frac{e}{2m}[\psi * (i\hbar\nabla + \frac{2e}{c}A)\psi + c.c.], \tag{2.11}$$

where $\nabla A = 0$, σ is the conductivity, μ is the scalar potential, A is the vector potential, e is electron charge, c is the speed of light, and m is electron mass. To help with stability, the Crank-Nicolson integration scheme and the linearization of the $|\psi|^2\psi$ term were done. An explicit integration would be subject to numerical instabilities.

2.9.2 Boundary conditions

There are two types of boundary conditions relevant to this system. They are quasi-periodic and open. On a quasi-periodic boundary, cells are treated the same as they would be in the middle of the system. The only thing that one needs to keep track of is the phase jump at the boundary. In other words, only the amplitude of the order parameter is really periodic. The open boundary refers to the Neumann boundary conditions. These mean that there is no current perpendicular to the boundary. Specifically;

$$\overrightarrow{n}(\nabla - i\overrightarrow{A})\psi = 0, \tag{2.12}$$

where $\overrightarrow{n}$ is the unit normal vector. For our studies, we stuck with quasi-periodic boundary conditions in the direction of current.

2.10 Results

Being such a general code, there were many possible areas of study regarding this code. We found promissing results in two general areas, grids of inclusions and super conducting-conducting funnels with higher T_c. We characterize these situations by looking at their responses to changes in voltage, magnetic field, and geometry. There is an important choice that we made when determining the critical current as there is a inherent hysteresis in the system. We had two options when ramping the current. It could either have been ramped up, Starting with no movement and pushing the current until the vortices became dislodged. The second option was to ramp the current down. That is start with moving vortices and slowly decrease the current until the vortices become lodged. In the end we went for the second option due to the dynamics of the system. Vortices tend to start out placed not according to the lowest energy state, but instead randomly according to whatever starting seed was selected. By forcing the vortices to move around first, we get a more natural state before the depinning current is found. In figure 2.5 we quantitatively demonstrate the difference.

2.10.1 Grids

Inclusions in the superconductive substrate can be used to contain vortices (up to a certain current). If these vortices do not move, then they are not draining energy from the system. The first thing we needed to show was that vortices preferred to be trapped in inclusions which were around the same size as they were. If the inclusion size is increased, we see that at some point we start to trap 2 vortices per inclusion. Trapping a vortex requires that the force due to external current and other vortices be less than the superconducting

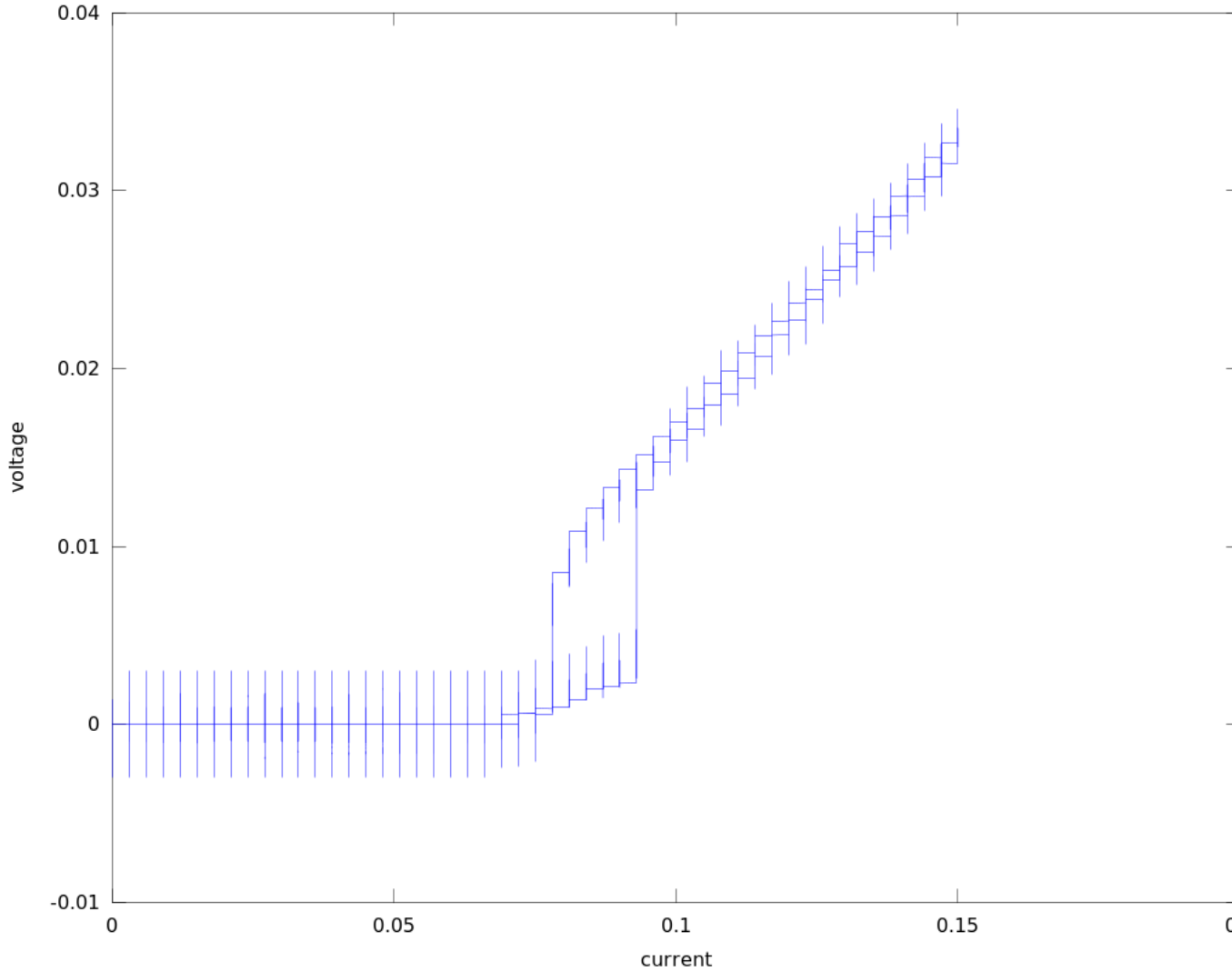

Figure 2.5: Overlapped are the current vs voltage for two systems, one with the current ramped up and one with the current ramped down. Upper one is the current being ramped down, while the lower one is the current ramped up.

destruction force. The superconducting destruction force is due to the energy of a superconducting system below Tc Being lower than a non-superconducting system below Tc. The second effect we were looking for was vortex matching resistance. Vortices have quantized magnetic flux. This means that for a certain applied field, we can predict the number of vortices. If some vortices are moving and some are pinned, the moving ones will push on the pinned ones as they pass by. If instead we have as many vortices as we have inclusions, after a certain relaxation period, vortices will all be pinned and the system will be more stable. As shown in Fig. 2.6 we were able to show both of these effects. In the X direction, we see that the optimal radius for an inclusion is 2. In the Y direction, we see a sharp drop in critical current at m=1. This is because as soon as we are above the 1-to-1 ratio, we start to have rogue vortices which will move. As the magnetic field is increased, we start to see that there islands of stability where multiple vortices can fit on the same inclusion. There is also a quadratic relation between the magnetic ratio and the size of the vortices in terms of optimal conditions.

2.11 Funnels

The same way that energy is gained when a vortex goes into a lower superconducting state, energy is lost if it tries to go into a higher superconducting state. Also, since more current can travel through the superconducting system, we get the opposite of the venturi effect. This also helps to keep vortices out. Using this logic, we created superconducting zones with higher T_c that can be used to guide vortices. Indeed, increasing the aperture size increases the ease of which the vortices can travel 2.21.

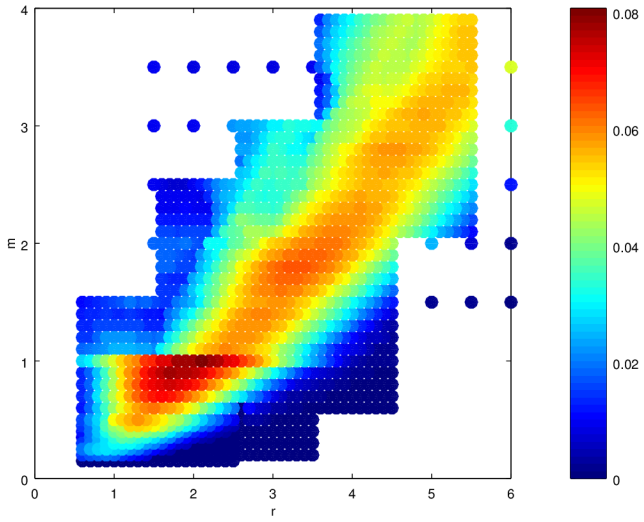

Figure 2.6: This is a superposition of 100+ simulations with different parameters. The critical current of each simulation was shown using color. On the X-axis is the radius of each inclusion in the system. On the Y axis m is the ratio of number of vortices per inclusion. The colorbar stands for critical current. In other words, the redder a zone is, the better it holds on to vortices, the higher the current can be before the vortices begin to slip.

2.11.1 Description

The magnetic field was kept such that the number of vortices filled 50% to 80% of the substrate. It was pointed into the board such that the current pushed the vortices into the funnel. The current was started at an amount large enough to guarantee vortex movement, even if it also meant that vortices went through the walls at first. The current was then slowly relaxed in enough timesteps to make sure that each configuration had enough time to stabilize. The number of current configurations had to balanced against practicallity. Ideally, we would use an infinite number of current configurations, but that would take an infinite ammount of time to simulate. Instead we tried to keep the simulation times at less than 24 hours.

2.11.2 Analysis

In general, the simulations performed as expected. The smaller the aperture, the better a system can hold on to vortices. This is up to a point which where even 1 vortex can no longer slip through. Steeper angles also improved the jamming performance of each system. The dependence did not seem to be linear in y-position of the funnel, or in angle. When looking at the magnetic dependence of the critical current, it is clear that more vortices increase the critical current of the system.

To conclude, we have explored multiple systems with the use of the GL program. We showed that if the number of inclusions matches the number of vortices, the system jams and we have much lower resistance due to vortex motion. We have also explored many funnel systems which are currently being tried out experimentally throughout the superconduction community. We showed that vortex jamming is a function of the angle of the funn el, the size of the aperture, and the amount of vortices.

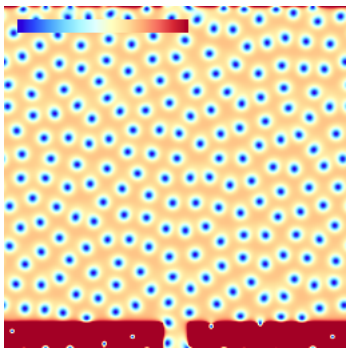

Figure 2.7: The amplitude of the complex order parameter. in yellow is the background superconductor, In red is the superconductor wall, and the blue dots are the vortices. In green is the parameter of interest. In this case, we have a flat obstruction which forces vortices through a narrow gap.

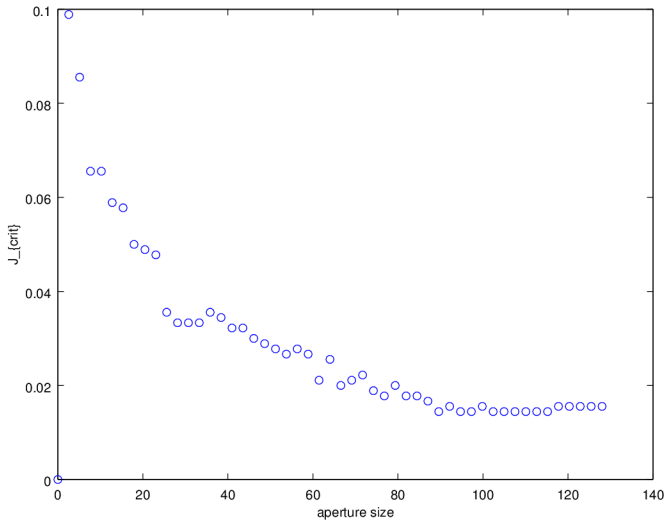

Figure 2.8: 50 values of aperture were run in this simulation. The resulting current was analyzed to find the critical current . As the aperture is increased, the ability to hold the vortices still is diminished.

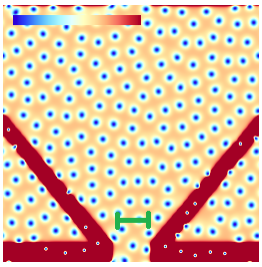

Figure 2.9: The amplitude of the complex order parameter. in yellow is the background superconductor, In red is the superconductor wall, and the blue dots are the vortices. In green is the parameter of interest. In this case it is the size of the aperture which was varied.

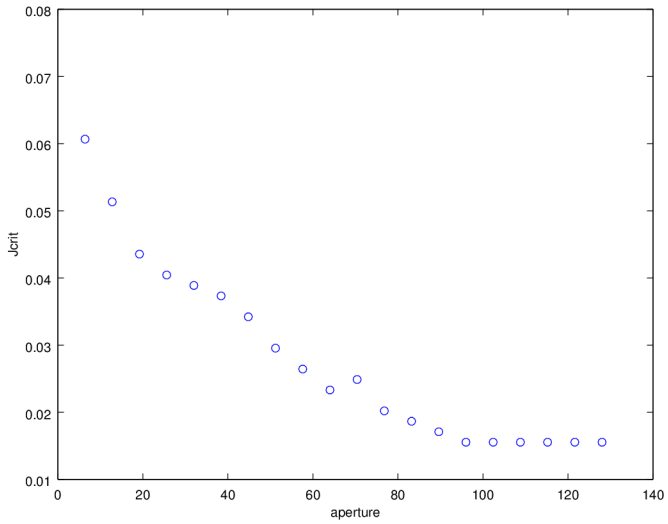

Figure 2.10: 50 values of aperture were run in this simulation. The resulting current was analyzed to find the critical current . As the aperture is increased, the ability to hold the vortices still is diminished.

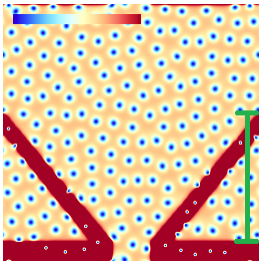

Figure 2.11: The amplitude of the complex order parameter. in yellow is the background superconductor, In red is the superconductor wall, and the blue dots are the vortices. In green is the parameter of interest. In this case it is the point on the Y-axis at which the funnel attaches and therefore the angle which varies.

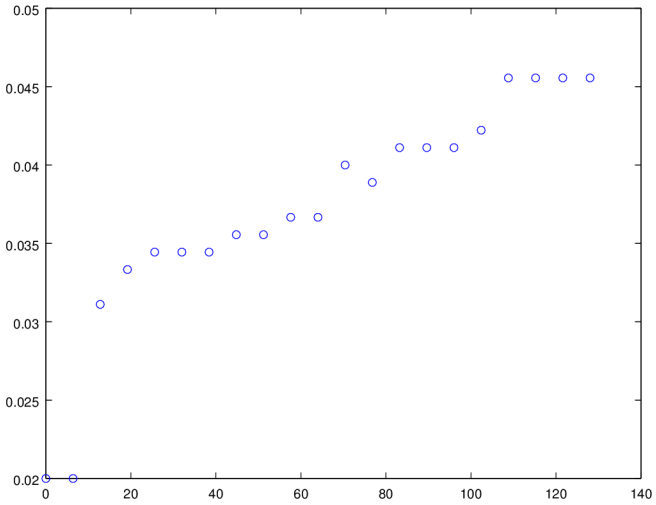

Figure 2.12: 50 values of aperture were run in this simulation. The resulting current versus voltage information was analyzed to find the critical current . As the angle of the slope is increased, the vortices were more easily jammed.

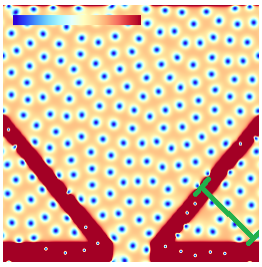

Figure 2.13: The amplitude of the complex order parameter. in yellow is the background superconductor, In red is the superconductor wall, and the blue dots are the vortices. In green is the parameter of interest. In this case the angle is held constant while the x and y attachments are varied.

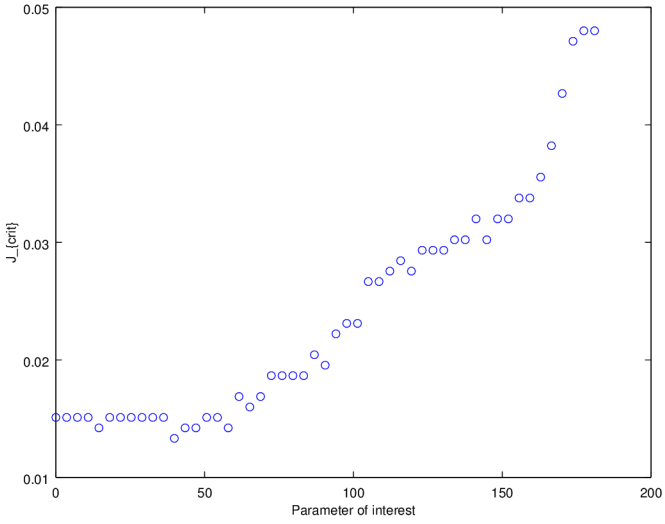

Figure 2.14: This is a scan of the parameter of interest versus the critical current. The x-postition and y-position of the funnel were moved uniformly as to keep the angle constant.

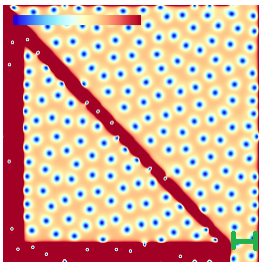

Figure 2.15: The amplitude of the complex order parameter. in yellow is the background superconductor, In red is the superconductor wall, and the blue dots are the vortices. In green is the parameter of interest. In this case it is the size of the aperture which was varied.

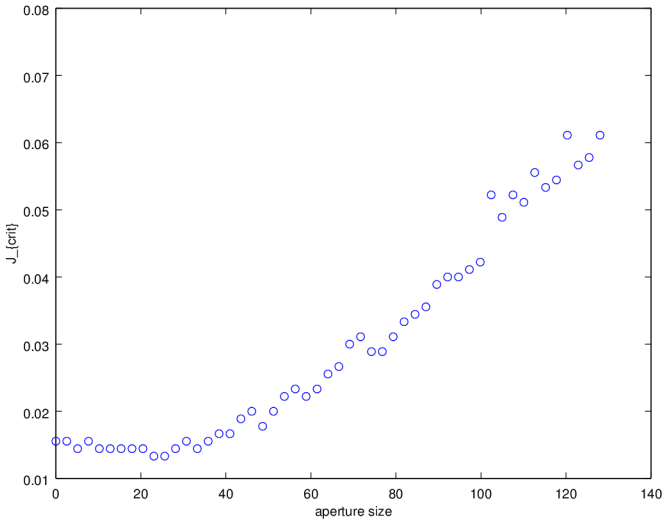

Figure 2.16: 50 values of aperture were run in this simulation. The resulting current versus voltage information was analyzed to find the critical current . As the aperture size is increased, the vortices are less restrained.

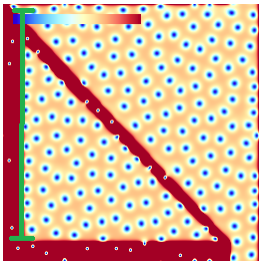

Figure 2.17: The amplitude of the complex order parameter. in yellow is the background superconductor, In red is the superconductor wall, and the blue dots are the vortices. In green is the parameter of interest. In this case it is the point on the Y-axis at which the funnel attaches and therefore the angle which varies.

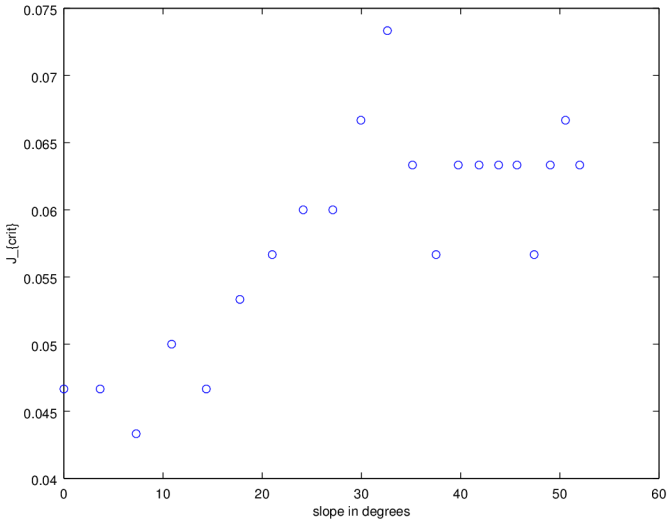

Figure 2.18: 50 values of aperture were run in this simulation. The resulting current versus voltage information was analyzed to find the critical current . As the one slope is increased, the jamming effect becomes more pronounced.

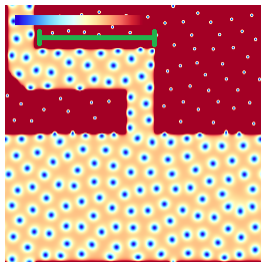

Figure 2.19: The amplitude of the complex order parameter. in yellow is the background superconductor, In red is the superconductor wall, and the blue dots are the vortices. In green is the parameter of interest. In this case it is the length of the "turn" which is being varied.

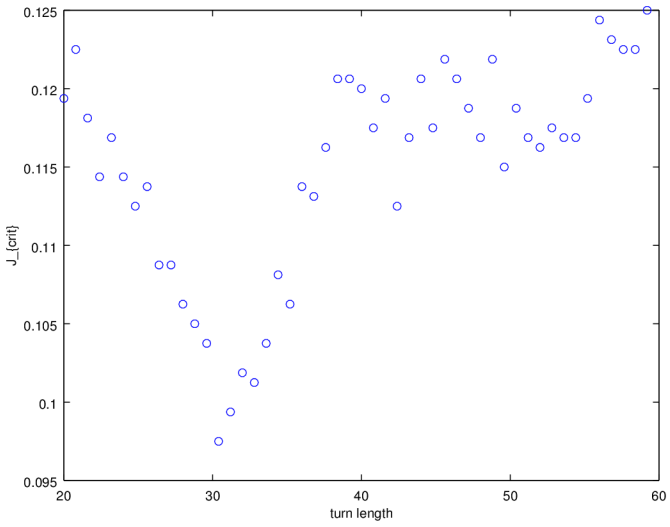

Figure 2.20: 50 values of the turn length were run in this simulation. The resulting current versus voltage information was analyzed to find the critical current .

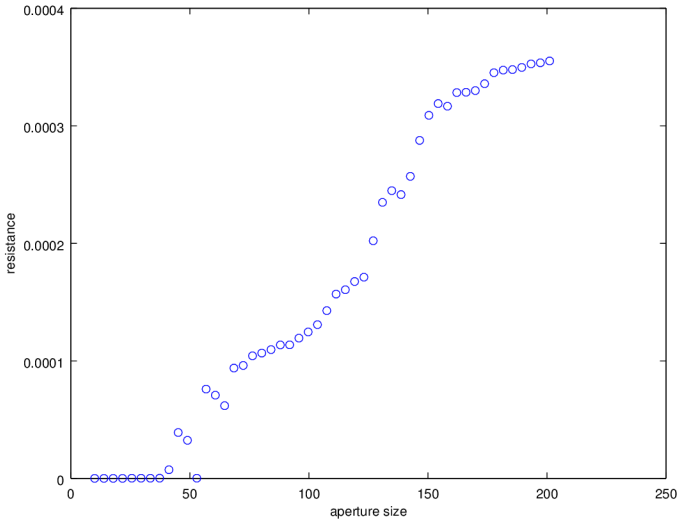

Figure 2.21: We can also study how the aperture size hampers vortex movement once they have already been depinned. This is a resistance plot of the constant y-position funnel. On the X axis is the size of the aperture, Y axis is the superconductive resistance.

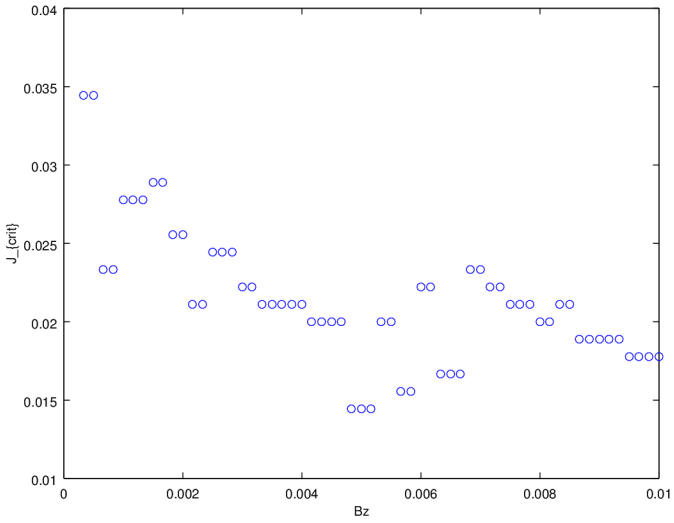

Figure 2.22: 50 values of the magnetic field angled system. The resulting current versus voltage information was analyzed to find the critical current .

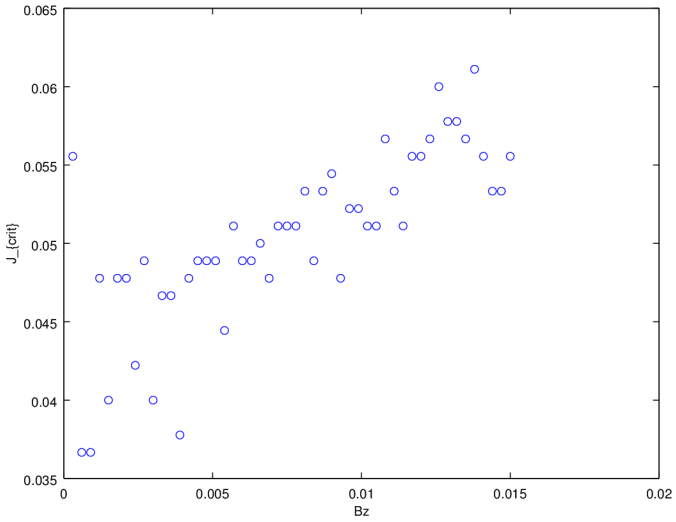

Figure 2.23: 50 values of the magnetic field were studied for the empty diamond system. The resulting current versus voltage information was analyzed to find the critical current .

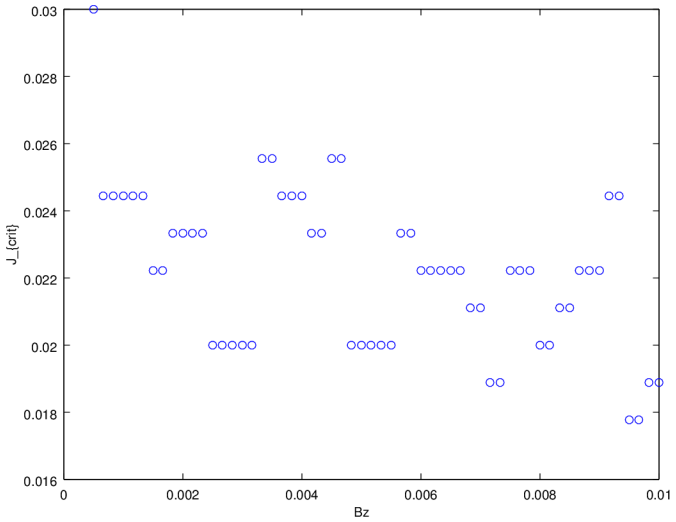

Figure 2.24: 50 values of the magnetic field were studied for the flat system. The resulting current versus voltage information was analyzed to find the critical current .

CHAPTER 3

VARIABLE RANGE HOPPING

3.1 Overview

In order to understand our work with DIAS, we must first go over a few seemingly disconnected topics. We begin by discussing the Monte Carlo method as it is the basis for our simulator. We then go on to discuss the physics of Coulomb glasses and how they relate to granular nanosolids. The point of this program is to simulate thermoelectric effects in granular nanosolids, so we will focus on thermoelectrics next. Finally we will be ready to dive into DIAS.

3.2 Monte Carlo methods

Monte Carlo methods are a randomized way to use the law of large numbers to find answers to mathematical and physical problems. For example, In oil and space exploration, Monte Carlo methods are a better predictor of cost overruns than human intuition [43]. While there is no consensus on the exact definition of a Monte Carlo method, One can get a feel for it by looking at simple examples. Some good examples are the estimation of π and the Metropolis method.

3.2.1 Estimating π

Estimating π has been a challenge for mathematicians since ancient Egyptian times. One possible method is by trying a Monte Carlo strategy. For simplification, one usually just takes a fourth of a circle inscribed in a square (see fig. **??**). One then picks random numbers between 0 and 1 for x and y. Success is then defined as [44]:

$$\sqrt{x^2 + y^2} < 1. \tag{3.1}$$

In a way, all we are doing is integration. If one counts the number of successes and divides by the number of total trials, it will equal to the ratio of the area of the quarter circle and the square of length 1, which can then be solved for π. Integration of this sort can be used to approximate the area under any integrable curve, and in the case of the "pathological equation" some non-integrable ones as well [**?**].

3.2.2 Metropolis method

The Metropolis algorithm is a way to draw samples from a probability distribution iteratively. Because each distribution is only affected by the previous distribution, this can be considered a Markov chain. A Markov chain is a sequence of random variables which a system moves through with serial dependence. In its simplest sense, we have

$$\vec{X}_{t+1} = \vec{\vec{Q}}\vec{X}_t, \tag{3.2}$$

where $\overrightarrow{X}_t$ is the state of the system at step t, and $\overrightarrow{\overrightarrow{Q}}$ is the probability matrix. Under certain circumstances, the probability matrix can be applied multiple times, eventually causing the state to approximate an equilibrium [45]. The Metropolis method can be used for many systems, but we will focus on the Ising problem as it is similar to our problem.

3.2.3 Ising problem

The Ising method is a way to solve the problem of dipole moments on a large array of atoms. While the Hamiltonian can be fairly straightforward (see Eq. 3.3), its properties such as its specific heat or hysteresis can be relatively complex. The Hamiltonian is

$$H(\sigma) = -\Sigma J_{ij}\sigma_i\sigma_j - \mu\Sigma h_j\sigma_j, \tag{3.3}$$

where σ_i is the spin, J_{ij} is the interaction strength between neighbors, μ is the magnetic moment, and h_j is an external magnetic field. Then the configuration probability is:

$$P(\sigma) = \frac{e^{-\beta H(\sigma)}}{Z_\beta}, \tag{3.4}$$

where $\beta = (k_B T)^{-1}$, and the renormalization constant $Z_\beta = \Sigma e^{-\beta H(\sigma)}$. From here we have a 3 step process to simulate the system. First, we must choose an arbitrary configuration to be our starting point. Next, we pick an adjacent configuration in configuration space (i.e. a configuration that we can get to by just changing one value). If going there is energy favorable, then the change is made. Otherwise, the change is made depending on the temperature. As the system is evolved, variables such as magnetic field and temperature can be changed, which can lead to properties such as specific heat and hysteresis.

Calculating the partition function (Eq. 3.4) in the thermodynamic limit involves doing an infinite amount of sums. The first step to simplifying this is to approximate the system on a lattice of finite size. Because of the dynamic complexity of even a small system (a 10 by 10 system can have 2^{100} configurations) simulations are a large part of modern electron hopping studies [4]. If we could sample 2^{45} of those sites on a good computer in a few hours, we would still miss out on the vast majority of states. This problem would be made worse at low temperatures where the system is dominated by a handful of ground states. Using a Monte Carlo system, we can find out which states will make important contributions to Eq. 3.4. There are however imporant conditions which must be followed when crafting a Monte Carlo system.

3.2.4 Conditions

There are certain conditions which an algorithm must comply with in order to be considered a Markov Chain Monte Carlo. The first is that the probability function should not vary over time. That is clearly satisfied as we stay in the form:

$$P = e^{-2R-\Delta E/T}, \tag{3.5}$$

where the probability of jumping is a function of the jump distance r, change in energy of the system E, and temperature of the jump site T. The second is that the probability to jump to the next state is only a function of the current state. In other words, there is no

"momentum" built up from previous states. Third is that the sum of the probabilities must equal 1:

$$\Sigma P(\mu \to \nu) = 1, \tag{3.6}$$

Where μ is the current state and this is being summed over all possible transitions to other states ν. Fourth is the requirement of ergodicity. That is, all states should be reachable from all other states given enough time. This requirement is satisified as long as there is at least one non-zero probability to jump out of every other state. Finally, our last condition is of detailed balance. That is, upon relaxation we generate the Boltzmann probability distribution rather than any other.

Kinetic Monte Carlo methods are useful when simulating condensed matter systems which include time evolution. There are two types, rejection and rejection-free, the difference being whether or not an event has a chance of failing all-together. If a kinetic Monte Carlo method is also subject to detailed balance, then it simulates a system at thermodynamic equilibrium [40]. A kinetic Monte Carlo method is useful for modeling variable range hopping. The temperature dependence of conductivity can be tested using a kinetic Monte Carlo algorithm.

3.3 Coulomb Glass

In 1937, Nevill Mott and Rudolf Peierls explained why some materials which should have been conductors, acted as insulators. This was due to electron-electron interactions, which is not taken into account in band theory [1]. From there, Miller and Abrahams proposed a network resistor model which Efros and Shklovskii built on [2]. The theory has gotten

more consise over time. For the sake of simulation, much of it can be compressed into equation 3.16.

Transport through a quantum dot which is weakly coupled to two conducting leads is dominated by the electron-electron interaction [38]. When the thermal energy is not enough to overcome the charging energy of the dot, Coulomb blockade takes over and resistance is increased. At low enough temperatures, the Kondo effect takes over. That is when the magnetic field of the electrons starts to matter energy-wise. At that point, electrons start to prefer states where they are anti-parallel.

If one assumes that single-particle excitations are responsible for variable range hopping, then one ends up with the Efros-Shklovskii law:

$$\sigma_c \approx (\gamma e^2/T)\exp(-(T_0/T)^{1/2}), \tag{3.7}$$

Where σ_c is the conductivity, γ is the frequency, T is the temperature, and $T_M = \beta_M(g_0 a^2)^{-1}$ where a is the localization length of the electron, g_0 is the density of states at the Fermi level, and β_M is a numerical coefficient. [39] show that single electron jumps are sufficient to describe the system. This is important since otherwise we would have to simulate multi-electron jumps which would scale the difficulty of simulation by an order of magnitude. The problem of studying this situation increases with decreasing temperature as electrons are able to jump farther.

The Coulomb glass system was found to be robust enough to relax within simulateable times. [?] Found that the relaxation time is slightly slower than exponential. Energy correlations at equilibrium however were found to be exponential:

$$C(\tau) = e^{-(\tau/\tau_0)^{\gamma}}, \tag{3.8}$$

where γ is proportional to temperature at low temperatures, and τ, τ_0 are time dependent. Only at low temperatures below $T_{min} \approx 0.02$ does the system take too long to equilibrate. The behavior is similar to that of a random walk on a fractal configuration space.

The Coulomb glass is applicable to nanoscale nanular lattices, and much research has been conducted on them. Abeles et. al. did some of the original work on nano-granules. They achieved this by co-sputtering metals and insulators. They attributed conduction due to electron percolation and tunneling. They also define a charging energy required to tunnel as $E_j = e^2/2C$ where C is an effective junction capacity. Another interesting phenomenon that they observed was that of the electric field breakdown. That is, if the voltage drop between particles became comparable to the height of the tunneling barrier, then electrons could go straight into the conduction band of the insulator.

In [15] The 2D lattice of Coulomb glasses with site disorder was studied. When the effect of site disorder was on the same scale as the Coulomb energy, the distribution of local minima becomes exponential. At low disorder, the density of states becomes crystal-like. They also found that in order to fully relax a system, multiple-electron jumps must be taken into account.

3.3.1 Density of States in a Coulomb Glass

There are many methods of characterizing the energy of an electron. One of these is the density of states. This is a histogram of the energies that electrons can be in. For example in 3.1, there are many electrons at a relatively low energy and the number of electrons with higher energies decreases with energy. In 3.3 there is only one energy option for electrons. We see two peaks because the holes act as particles in that the system requires energy to move those as well. The value on the x axis is the energy required to fill or empty each

hole or particle respectively. By knowing the shape of the density of states, one can discern important intricacies of a system. These can include the energy scales, the relaxedness, and the bandgap of a system. If the particle distribution is symmetric (same amount of electrons as holes) then the density of states will be symmetric, as long as the system is relaxed [26].

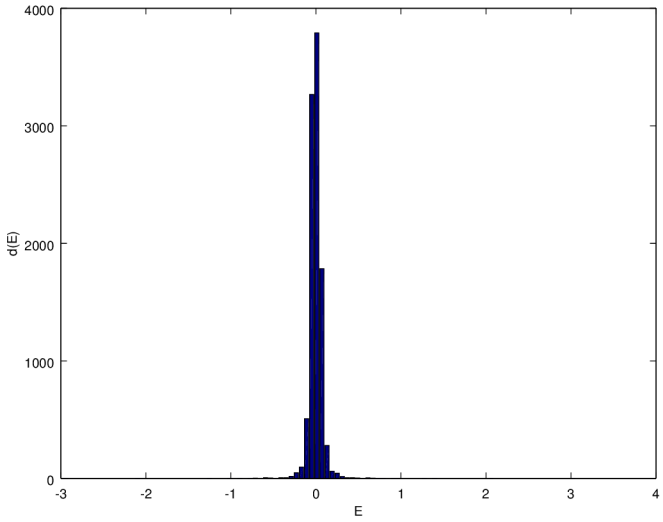

Figure 3.1: The density of states for a system with a high amount of randomness in the energy.

3.3.2 Comparing Mott VRH against Effros-Shklovskii VRH

While the approach to describe physical systems by Mott vs Effros-Shklovskii (ES) theory are similar, there are a few key differences in the details. First, The localization parameters are different due to differences in the density of states. The localization is temperature dependent in the ES system. This is because ES considered the situation where if an electron tries to tunnel, It must leave an electron hole behind. This enhanced requirement for the

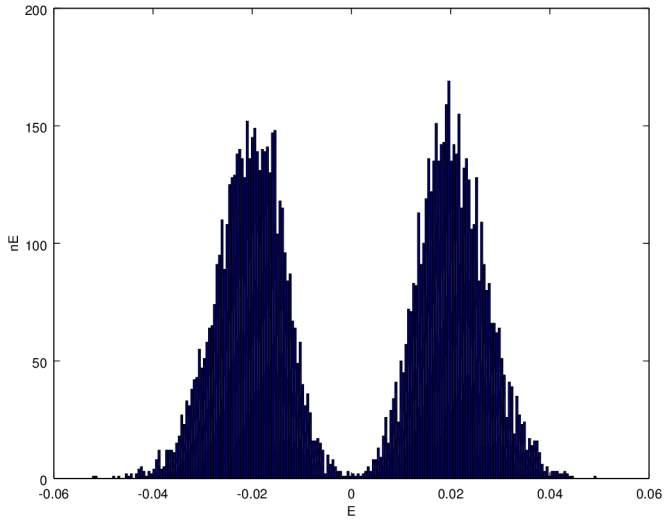

Figure 3.2: The density of states for a system where there is a critical amount of randomization and the two peaks are just beginning to touch.

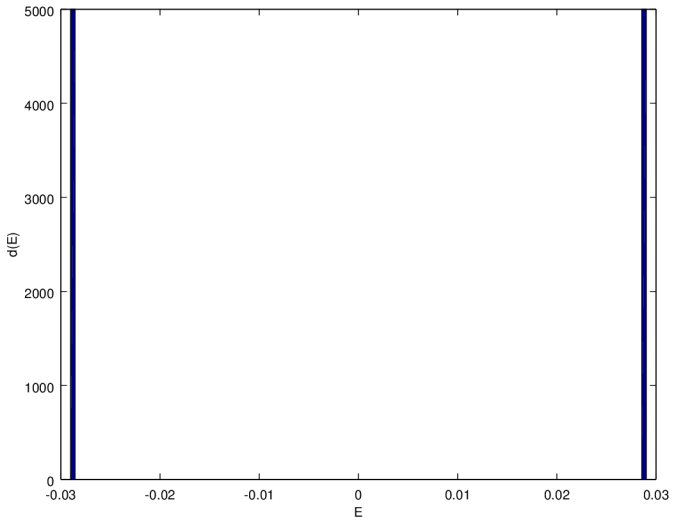

Figure 3.3: A low entropy system (Wigner crystal).

energy means that at low temperatures, the density of states at the Fermi level vanishes [6]. The resistivity for the Mott system ends up being related to the temperature as

$$\ln(\rho) \approx (T_o/T)^{1/4}, \tag{3.9}$$

where ρ is the resistivity and T is the temperature. Meanwhile, in the ES system we have

$$\ln(\rho) \approx (T_o/T)^{1/2}. \tag{3.10}$$

The Mott resistance comes from $\delta E = \alpha_1/gr_{ij}^3$, where α_i are prefactors of order unity. The ES resistance comes from the usual Coulomb blockade term $\delta E = \alpha_2 e^2/\kappa r_{ij}$ [5]. The Differences can be summarized in a single plot 3.4 [14].

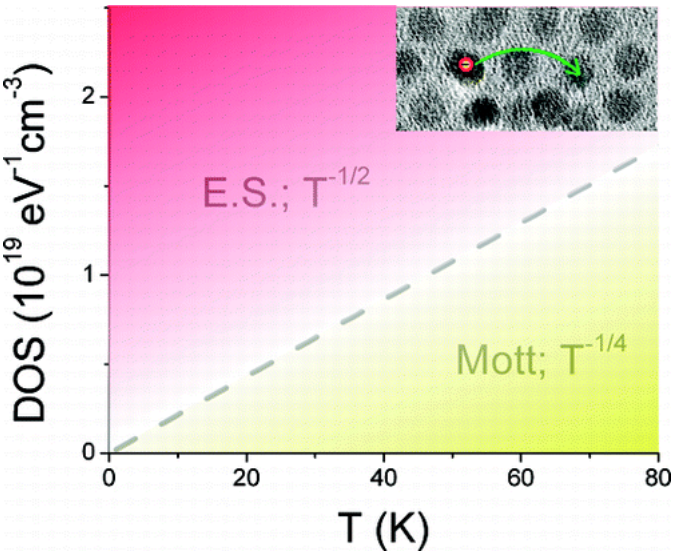

Figure 3.4: Density of states vs Temperature. This plot describes the interface between ES and Mott transmission of electrons. (Graph courtesy of Heng Liu)

3.4 Artificial Nanosolids

In a sense, artificial nanosolids are like hyper-Coulomb glasses. They have many of the same attributes if one treats each atom as a granule. Each granule consists of thousands of atoms, yet is small enough to observe the Coulomb blockade. They are also known as granular films and can be prepared by co-sputtering metals such as nickel and gold with insulators such as silicon dioxide or aluminum oxide. Strong electron scattering from dielectric inclusions or grain boundaries. Electrical transport will typically occur via tunneling between granules. Intra-grain conduction is significantly higher than inter-grain conduction and so is typically ignored. Depending on the type of material (conductors, semiconductors, insulator), the energy levels inside the granules can be tuned. The size of the granules also plays a large role in determining the energy levels [42]. These metallic particles act like artificial atoms with programable electronic properties. These can be formed such that they are insulators, conductors, semiconductors, or even superconductors. Beloborodov et. al. [17] Were able to show that there was logarithmic temperature dependence of the conductivity. This system also appears to show negative magnetoresistance under certain parameters.

By tuning the ability of electrons to travel, one can also start to change the Seebeck coefficient of the material [**?**]. The Seebeck coefficient gives us a general idea of the performance of the artificial nanosolid. Glatz et. al. derive the thermopower and thermoelectric coefficient of nanogranular materials. They find the thermoelectric coefficient to be:

$$\eta = \eta^{(0)}(1 - \frac{1}{4g_T d} ln \frac{g_T E_c}{T}), \tag{3.11}$$

where $\eta^{(0)} = -(\pi^2/3)eg_T a^{2-d}(T/\epsilon_F)$, a is the size of a grain, d is the dimensionality of the system, ϵ_F is the Fermi energy, and $E_c = e^2/a$ is the charging energy.

3.4.1 Inelastic vs. Elastic tunneling

As well as blocking each other, electrons also can impart energy onto each other which may result in an electron being dislodged. This is referred to as inelastic co-tunneling. If instead the electron tunnels or otherwise travels without dislodging, it is referred to as elastic co-tunneling (see fig. 3.5). For low to medium temperatures, the main tunneling mechanism will be elastic. At higher temperatures, we expect a transition to in-elastic tunneling [38].

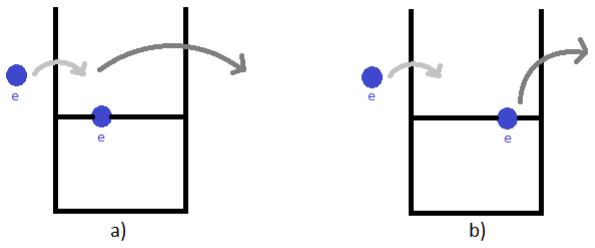

Figure 3.5: a) elastic transmission of electrons. b) inelastic transmission of electrons.

3.4.2 Coulomb Glass vs Artificial Nanosolids

Coulomb glasses are the original substrate on which the ES model of electron conduction was based. The "glass" in Coulomb glass refers to a phase in which electron-electron interactions impair conduction and dynamics become slow, like the flow of a glass [9]. Artificial nanosolids are arrays of granules which have a higher intra-granule conduction than a inter-granule conduction. The differences begin at the density of states. In artificial nanosolids, the density of states can be more creative. By changing the size of the granule, and the material it is made out of (metal, insulator, superconductor) the amount of available electron

slots per site (and the energy of each slot) can be chosen. There are two energy scales for each grain. δ is the mean level spacing. E_c, the energy required to pack on one more electron onto a site is on the order of 3000 Kelvin [11] .The distances are also different. For Coulomb glasses, the distances are basically the inter-atomic distances. There we are basically talking about electron jumps between atoms on a crystal lattice. As the name suggests, in artificial nanosolids the distances are nanoscale and tuneable. For typical artificial nanosolid applications, we are in the nanometer to tens of nanometers range [10]. While the general electric potential plays a role in both systems, It plays a bigger role in the Coulomb glass since the scales are smaller and the electric potential scales as $1/r$. Before we get too far into the practical applications of artificial nanosolids, we must first discuss thermoelectrics.

3.5 Thermoelectrics

Thermoelectric devices are a way to get electrical energy out of thermal gradients or vice versa. The problem is that electrons which conduct electricity also conduct most of the heat. Materials which tend to be good electrical conductors also tend to be good thermal conductors. This conundrum is refered to as the Wiedemann-Franz law [7].

There are two governing variables in thermoelectrics, device efficiency and power factor.

$$\eta = \frac{E_{in}}{E_W}, \tag{3.12}$$

where E_{in} is the energy put into the system, and E_W is the heat pumped to the hot end. The power factor for a thermoelectric is:

$$P = \sigma S^2, \tag{3.13}$$

where σ is the conductivity.

The number that denotes usefulness of a thermoelectric device is the dimensionless figure of merit

$$ZT = \frac{\sigma S^2 T}{k}, \tag{3.14}$$

where σ is the conductivity, S is the Seebeck coefficient, T is the temperature, and k is the thermal conductivity [8]. The Seebeck coefficient is a relationship between the electric gradient and the thermal gradient:

$$S = \frac{V}{\Delta T}, \tag{3.15}$$

In order to have optimal conditions, phonons must see the substrate as a glass, while electrons see it as a crystal [48]. Each granule in the Coulomb glass-like material acts to scatter phonons. If a semiconductive lattice of granules is interspersed with conductive granules, then tunneling electrons will effectively see a crystal. With this understanding of the physics involved, we wrote DIAS.

3.6 DIAS

3.6.1 Algorithm Parameters and Choices

DIAS (Dynamics In Artificial Solids) is a code which at its heart is a 2D Monte-Carlo simulator. DIAS begins by taking in parameters such as granule-to-granule distance, number of electrons, number of lattice sites, number of time-steps, temperature, voltage bias, thermal gradient, material coefficient, and substrate potential variance. The granule-to-granule dis-

tance is on the order of 10 nanometeres. We have a square grid which is periodic. Variances in granule distances are uniformly introduced with limits according to user-set parameters. The number of electrons can vary between double-empty systems and double occupied sites. The number of time-steps is usually set to the square of the number of particles. This is to ensure a statistically justified result from the monte carlo aspect of the simulation. Temperature is set in Kelvin and is usually varied in the range where our material coefficient would give interesting results. A positive voltage bias will act on a particle so that it is coerced to move upstream. Conversely, a positive voltage bias will force a hole to move downstream. This hints at a particular symmetry in which we chose for the simulation. Some previous studies have chosen to only focus on electron jumps and reject any jump that begins with a hole [19]. We decided to allow jump probabilities to be calculated from an electron hole's point of view as well. For current/voltage measurements, the system is periodic so that the current will just keep traveling at a steady pace. A second version of the code was created where the boundaries formed a closed system to study thermoelectric properties. The memory choices we made are also worth mentioning. There were several arrays of data and keeping these to a minimum was important as memory management was an issue due to the limited space on GPU cards. These matrices include particle/hole, substrate potential, distance between sites, thermal gradient, and size of each granule. In order to maintain neutrality, the voltage bias was artificially set. This meant that the effective charge of a filled site was half an electron. If an electron were to move, the charge then became negative half and electron. The Monte-Carlo algorithm shows up twice to find the jump site.

3.6.2 Algorithmic Strategy

First, a lattice site is chosen with probability according to its energy. Second, the jump probabilities to each site are calculated using Eq. 3.16 for said site. We do not allow jump probabilities greater than $L/2$. In fact, the system is periodic, so anything past $L/2$, is actually closer than $L/2$ in the other direction. These probabilities are summed up and a number is chosen between 0 and that sum. This in turn gives a Monte-Carlo jump which is weighted by the jump probabilities. This jump is done and the system moves on to the next timestep under the new electron configuration. Meanwhile the properties of interest are measured. This repeats for the number of requested time steps. Originally we picked the starting particle randomly. Unfortunately in order to have a rejection-less system, this cannot happen. If it did, then particles which would have practically no chance of jumping would be moved with probability $1/N^2$, the same as any other particle. In order to fix this, we followed the algorithm posed in [21]. They propose first picking two particles with probabilities via the tower method, based on their energies. This way, particles which are less stable are moved more often. Because of the distance parameter in our probability, we are forced to pick one particle at a time. This way the second particle is picked based on the change of energy of the system, with a distance component. This algorithm allows for maximum parallelization and no rejection. The parallelized tower method is efficient as we can use a parallel prefix scan to stack the probabilities while also finding the maximum value in order to normalize. Doing a search for the right interval can also occur in parallel as each thread can be given a range, and the appropriate range can be found in log(N) time.

3.6.3 GPU Algorithms

Electron hopping via Monte-Carlo algorithm can be solved particularly efficiently using parallel/GPU algorithms. Specifically we use an algorithm called the "tower method" [20]. Typically when one is doing a Monte Carlo study, there is an acceptance region and a rejection region ammong a range of choices. A choice is examined and it is either rejected or accepted. Using the tower method, all choices are stacked on top of each other (like a tower) and there is no rejection region. The first step, finding the probability to jump to each site is solved via the classical parallel scheme, where each lattice site can be individually calculated in its own thread. Once we have the probability matrix, we need to sum it in order to normalize it. This can be done via a parallel reduction algorithm. Taking advantage of on-board GPU memory, we can perform the reduction in O(N/P + log N) time rather than O(N) time, where P is the number of GPU cores. Now that the system is normalized, we can roll a dice between 0 and 1 to find where the particle will go. We must then sum our probabilities until we find that number. This can be done with a parallel prefix sum. Parallel reduction and prefix sum algorithms were written and then replaced by Nvidia's more efficient Thrust functions. Thrust is a template library for CUDA which allows the implementation of high performance parallel applications. Each choice of substrate and position randomization has its own ground state. This ground state is found through a relaxation algorithm.

1: First a nearest neighbor exchange
2: **for** n = 1 to number of sites **do**
3: **if** there's a particle at that site **then**
4: calculate energy without moving the particle:
5: *potential energy calculated everywhere*
6: *sum reduction of the potential energy to one number (lets call it S_1)*
7: test moving the particle up
8: *potential energy calculated everywhere*
9: *sum reduction of the potential energy to one number (lets call it S_2)*
10: **if** $S_1 > S_2$ **then**
11: leave the system
12: **else**
13: change it back
14: **end if**
15: repeat for the other 3 directions (down,left,right)
16: **end if**
17: **end for**
18: The system is now slightly more relaxed
19: Now for switching highs and lows
20: **while** system is not relaxed **do**
21: **for** n = 1 to number of sites **do**
22: find the energy at each site normally:
23: *calculate potential,substrate, & coulomb blockade energy everywhere. Sum and call this S_3*
24: find the energy at each site with the particle removed (or added if the site was empty):
25: *calculate potential,substrate, & coulomb blockade energy everywhere. Sum and call this S_4*
26: DosMatrix[n] = S_4 - S_3

Another part of this algorithm that is important to understand is the "Tower Method" and is integral to a kinetic Monte Carlo algorithm. It is used in picking the starting particle as well as picking the particle to jump to.

```
1: Total = 0
2: for n = 1 to number of sites do
3:     Total =+ P_n
4: end for
5: newSum = 0
6: pick a random number R from 0 to Total
7: for n = 1 to number of sites do
8:     newSum =+ P_n
9:     if newSum > R then
10:        stop For loop, current i is the jump site
11:    end if
12: end for
```

Another way of thinking about this is by spinning a "wheel of fortune" style wheel where each slice's size is proportional to the probability.

The following pseudocode is what is referred to as the "Parallel Reduction". It is device specific to GPGPU's, but can be generalized depending on "shared memory". If generalizing, the maximum number for "shared memory" is equal to the number of processors available. This can be easily combined with a simple parallel sum to create a parallel dot-product algorithm. A similar algorithm can be used to efficiently determine the maximum or minimum number of each array. This time instead of placing the sum of the two numbers, one can place the larger of the two numbers. This algorithm can repeat until the largest number is found.

```
1: number of slices = sizeArray/sharedMemory + 1
2: size of slice = sharedMemory
3: sumStart = 1
4: for i = 1 to number of slices do
5:     for k = 1 to log(size of slice) do
6:         for  j = sumStart to size of slice/2 do
7:             add first half of slice to second half, put that sum in the second half
8:         end for
9:         sumStart = size of slice/2
10:        size of slice = size of slice / 2
11:    end for
12: end for
13: (now we stitch each shared memory together)
14: totalSum = 0
15: for i = 1 to number of slices do
16:    totalSum = totalSum + sliceSum
17: end for
```

Many parallelized algorithms tend to take a "power of 2" strategy.

3.6.4 Jump Probability

In order to calculate the electron variable range hopping (VRH), we must first find the probability of each jump site. Our main equation involved is as follows:

$$P_{ij} = \exp(-2\alpha R_{ij} - E_{ij}/kT) \tag{3.16}$$

where k is the Boltzmann constant, R_{ij} is the distance between cells, E_{ij} is the energy change of the system if a particle were to move from i to j, and T is the temperature of the system.$\alpha = \sqrt{2mH/\hbar}$ where m is the effective mass at the bottom of the conduction band and H is the mean energy of the conduction band. α is set up to be around the same scale as the inter-grain distance. E_{ij} has various inputs which vary in energy scale [37].

$$E_{ij} = \triangle U_{ij} e^2/a\kappa_1 + e f_i \triangle V_{ij} + f_i \triangle \mu_{ij} + f_i(eV)\triangle x_{ij} \tag{3.17}$$

where i refers to the starting site index and j refers to the target site index, f is the occupation of a site, a is the size of the granule, κ_1 is the intra-granule dielectric constant, μ is the substrate potential, $V_{ij} = \sum_{i,j=1}^{N} e^2/\kappa_2 r_{ij}$ is the local potential from the rest of the particles, κ_2 is the inter-granule dielectric constant, $\triangle x$ is the component of r in the direction of eV , and eV is an externally applied voltage. $\triangle U_{ij}$ is the difference in charging energy. The first two components of equation 3.17 together constitute the electrostatic component of this system. The most powerful is the Coulomb blockade. This introduces a large penalty into the probability of an electron occupying the same site as another electron. If the site at which an electron can travel to is empty, the chances of transport are higher than if the site is filled [3]. There is also a contribution from the substrate. There is an inherent randomness in the potential at different lattice sites and that is where this comes in. This energy landscape somewhat randomizes starting energies and can fill in as electron donor. There is a general electric potential which will try to get the electrons to space out evenly in the substrate (periodic boundary conditions). Finally there is a current portion which if a voltage bias is applied on the left and right sides of the system, then the probability of electrons hopping with that bias is increased [5]. The exponential term is artificially limited below 0 to keep the electron hop ranges realistic. Analytically, equation 3.16 can be maximized to find the most common jump distance (take the derivative with respect to

r and set equal to 0). In our case, there are 2 problems with this approach. First, we are more interested in the average jump distance which need not be the maximum. Second, The analytical approach assumes a continuous system, where in reality it is a discrete number of interacting points.

3.6.5 Optimizations

Various optimizations were done in order to speed up this code. Originally this was a linear CPU code, but obvious parallelisms made this code perfect for being run on a GPU. Still, there were some less obvious optimizations. One such optimization was previously discussed, moving to a rejection free system. In a rejection system, the particle has a high chance of staying at the same cell each turn. This means that a lot of computation is spent not gaining any valuable information. To fix this, we moved to the rejection free system (BLK?) [21]. It is as if one jumped the simulation forward skipping all non-events. For one to do this, the system time must be kept. This is done by integrating all of the probabilities:

$$\delta t = \frac{1}{\Sigma P_{\mu \to \nu}}, \tag{3.18}$$

where δt is the change in system time, and $P_{\mu \to \nu}$ is the Markov transition matrix. Because of CUDA and algorithms like parallel reductions, it ends up being much faster to calculate this than to try to calculate all of the rejections. There were optimizations that skipped unnecessary calculations. One of these was the calculation of the potentials after a particle is moved. The naive way to do this would be to recalulate all of the potentials from each particle. The optimized way to do this would be to use a crater-mound system. That is, only focus on the effects due to the particle that has moved. In other words, calculate the difference on the potential that taking that one particle away would change and calculate

the sum on the potential that adding a particle would cause. Using a 4D lattice matrix also saved simulation time at the expense of system memory. This matrix held the distances of every particle with respect to every other particle. Technically this matrix only had to be $N^4/2$ in size, but making it N^4 simplified the already ardous task of using a 4D matrix and was faster than an algorithm which could operate on a $N^4/2$ matrix.

3.6.6 The Lattice

While the easiest system to model would have been a square lattice, This would have left out a large amount of interesting phenomena. To incorporate this, we started out with a square lattice and then gave each site a certain δx or δy variance. There are a few ways to then use this kind of implementation. The first one would have been to then calculate the distances from one site to another on the fly, possibly approximating for further away site. The way that we picked to do this was to hold all of the distances from one site to another in a 4D matrix (a matrix of distances for every site on the grid). This has the advantage that no calculations have to be run at each GPU core. Since the calculation of distance involves a square root, this would have been heavy on the workload. The disadvantage is that for a 100×100 system, we require $100 \times 100 \times 4$ bytes of data (or 400MB using the float type). Fortunately, NVIDIA GTX 570 cards have at least 1200 megabytes of memory, so this did not end up being an issue.

3.6.7 Continuous Time

There seems to be a lot of disagreement on how to measure the time in a Kinetic Monte Carlo algorithm. [19] chose to go with the system where δt was sampled randomly from a

Gaussian distribution of mean m/Γ and standard deviation $\sqrt{m}/\Gamma$ where $m = pM+q$ and p is the number of iterations since the previous successful step. On the other hand, [41] rigorously establishes a physical time scale for kinetic Monte Carlo algorithms. He finds the master equation for time step length to be $\delta t = -ln\xi/w_i$ where ξ is a uniformly distributed random variable between 0 and 1, and $w_i = \Sigma_{j\neq i} = r_i/\nu e^{-\beta\Delta E} b_i$, $r_i = \Sigma_{j\neq i}\nu e^{-\beta\Delta E_0^m min(e^{-\beta(H_j-H_i),1})}$. Finally we went with the simplest solution provided by [21], eq.3.18.

3.6.8 Dielectric Constant

We also varied the dielectric constant of the material. Typical dielectric constant was held at around 4. For gold nanoparticles, this number can be higher. While gold is a conductor and conductors tend to have a dielectric constant of infinity, these gold nano-particles are in a very special situation. First, they are small, so there are skin-level effects which mean that while the interior may want to reach a high dielectric constant, the skin still has a finite constant. Second, The dielectric constant of gold varies with frequency. It may be infinite for a static field attempting to permeate through a block of gold, but different frequencies will feel different impedances. We approximated the effects of varying the dielectric constant by taking the geometric average of the two interacting lattice sites.

3.6.9 Distance-substrate correlation

In the physical world, this system is not a grid, but rather a dense packing of granules. This can be imagined as a 2D packing of variously sized orbs. One can then see that the distance between orb centers will depend on the size of the neighboring orbs. For ease of algorithms, we took this correlation in the opposite direction. The size of an orb is defined

by half the distance to the nearest orb. The substrate potential is also affected by this. Granule size randomness did not have much effect on the system directly. This is because it only affects how much energy it takes to pack two electrons on the same granule. If the granule is bigger, the electrons do not have to sit so close together and the charging energy is lowered. But the issue is that even with a larger granule, the temperature required to pack two electrons onto the same granule is still in the thousands of Kelvin and outside of the scope of this study. The correlation's effect on substrate randomness however did come into effect, as small changes in the substrate potential can have large effects on the density of states.

3.6.10 Temperature

Temperature-dependent phase transitions are scattered throughout the spectrum and so it is important to specify at which temperatures we are working with. At temperatures lower than the Neel temperature, We encounter the first transition called "Mott-Heisenberg". At these low temperatures, the magnetic fields of the electrons have a chance to couple into anti-ferromagnetic pairs. Also, During tunneling events, electrons will avoid atoms which are occupied with other electrons of similar spins as sharing an atom would require an increase in energy compared to one of opposite spin [12]. At medium temperatures, we have a transition between elastic and inelastic. In order for an electron to land on an occupied site it must have enough energy to overcome the Coulomb blockade. This is only possible if it was given enough kinetic energy from a phonon (sufficient thermal energy). As the temperature is increased, electrons can begin stacking. Once an electron stacks onto another electron, Coulomb repulsion guarantees that either electron will quickly move on [38]. At much higher temperatures, the system starts to have enough free thermal energy to exceed the Coulomb

blockade energy. That is, the energy required to stack 2 electrons in the same quantum dot. This yields a crossover temperature which was discussed during our comparison of ES vs Mott systems [5]. Depending on the density of states, there will eventually be higher energy states on which to pack on electrons. For our purposes, we will stay in between these two systems. Our temperatures will be high enough that magnetic moments can be ignored, yet low enough that the maximum number of electrons allowed on the same quantum dot will be two. There are a couple of important temperature-dependent effect which we show with our simulations. At low temperatures, tunneling occurs more often and so particles have a further jump distance. At high temperatures, the energy-related effects are suppressed and only the distance related tunneling effects remain. This means that at high temperatures, we expect jumps to be restricted to nearest neighbors. One would think that this effect would cause conductivity to be high at low temperatures and low at high temperatures, but the opposite is in fact true. That is because of the second temperature related effect. That is at low temperatures, the chances of a jump happening in general are much lower than at high temperatures. In other words, At low temperatures we have a few large jumps while at high temperatures we have many short jumps.

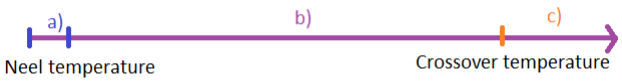

Figure 3.6: Neel temperature and charging temperature are material dependent, yet the former tends to be in the sub Kelvin range and the latter tends to be in the thousands of Kelvin.

3.6.11 Density of States in DIAS

The energy involved when removing or adding a particle to a lattice site is what determines the probability to jump to it. It then makes sense to ask what the distribution of potential energies will be. The purpose of this code was not originally to determine the density of energy states of an electron lattice. Nevertheless it serves two practical purposes. First, it helps to make sure that the particular energy contributions are balanced accordingly. Looking at the density of states, one can immediately associate characteristics to electrical potential, substrate potential, etc. Then, at a glance, one can quickly determine if the substrate potential is too strong and is washing out electric potential contributions. The second purpose is to assure that a particular system is fully relaxed before simulations begin. Due to the inherent randomness of the system, particular outcomes may sharply vary depending on the initial conditions. Assuring that the system is relaxed before starting can compensate for this. One clue that the system is relaxed is that in two dimensions, there will be a linear (absolute value) pattern near 0 in the density of states. We use a previously determined algorithm in order to quickly relax our system [15]. We begin with a nearest-neighbor comparison of every particle site and moving them if the overall energy is lower. Then we find the particle which is imparting the most potential energy by existing. This is compared to the hole for which filling it would cause the most potential energy to be added to the system. If the two energies, when summed, are less than the original, then the switch is performed. The area around each switched particle is then scanned to see if any readjustments can be made to further lower the potential energy of the system. The density of states is then measured again everywhere and the process is repeated until the energy can no longer be reduced. The valley in the density of states can also be characterized. If the slope near $E = 0$ is linear, then we know we are looking at a 2D system. If it is parabolic,

then this signifies a 3D system. As a benchmark, we analyzed our valley slope and found it to agree with the 2D system characterization.

3.6.12 Thoon Cluster and Computational Resources

This research was performed on a variety of machines, mostly consisting of Nvidia graphics cards. I had access to one stand-alone pc with a GTX 570 graphics card, 8 pcs in a computer lab with GTX 570s, and 60 nodes with 2 GPU's each on the Gaea cluster in the computer science building. The Gaea cluster was powerful, but frequently busy such that only a third to an eighth was typically available. Meanwhile there was a computer lab with 8 linux based pcs, each with an Nvidia gtx 570. Unfortunately, they were barely on the same network. To remedy this, I wrote a script which divided up the parameter scans in the form of bash scripts and sent these to the respective computers. These then started the simulations and a timer in the form of a cron argument. The cron would then check every five minutes to see if the simulation was done. If so, then the data was sent back to the host computer. This had a few weaknesses, namely the clunkyness and the fact that one had to wait for the cron to trigger. This meant that short scans were impractical. Eventually this was all replaced with the free-lisence version of the Torque job scheduler. With the computers united into a small "cluster", running batches became more streamlined. This ad-hoc cluster is called THOON (Torque Hub On One Node). The cluster uses a network file system to share data in between the computers.

3.7 Results

3.7.1 Algorithmic Benchmarking

The average jump distance for a high temperature system should be 0.69614 spaces. This matches to within 1% accuracy with my results of 0.68943 spaces. This difference is negligible considering the statistical variation of any Monte Carlo system. The expected jump distance was found via Monte Carlo integrator. First, the values of Eq. 3.16 were found at a grid of points with similar spacing to what we use in the simulation. Second, particles were dropped onto this grid depending on the function values a-la Monte Carlo method. Third, the mean jump distance was calculated via the first moment equation

$$\bar{r} = \frac{\sum r \cdot n}{\sum n}, \tag{3.19}$$

where r is the distance from the center of the grid cell, and n is the number of particles at each grid cell. The parameters for this comparison were fairly basic. The temperature was 1 degree kelvin, there was no external current, the system size was 100x100, and there was only one particle. Multiple particle comparisons have been done, but because the jump probabilities are different depending on wether the site is empty or full, the comparison becomes much more complicated. The point of this benchmark was to make sure the complicated GPU Monte-Carlo integrator was working as expected. With 3 major components to this system, (calculating the energies, calculating the weights from the energies, and calculating a jump site from the weights), this was a simple way to make sure everything was working together properly. Creating simple scripts to test more complicated scripts also became a useful tool in other parts of the research. For example, studying the behavior of the energy as

a function of distance can be done via the Dias simulator, and outputs can be output for testing. But this can be complicated and the program may need to be changed and re-compiled in between tests. By writing a simple function in Octave and tuning the same parameters, the interaction between different energy sources could be observed more closely.

3.7.2 Algorithmic Benchmarking

The average jump distance for a high temperature system should be 0.69614 spaces. This matches to within 1% accuracy with my results of 0.68943 spaces. This difference is negligible considering the statistical variation of any Monte Carlo system. The expected jump distance was found via Monte Carlo integrator. First, the values of Eq. 3.16 were found at a grid of points with similar spacing to what we use in the simulation. Second, particles were dropped onto this grid depending on the function values a-la Monte Carlo method. Third, the mean jump distance was calculated via the first moment equation

$$\bar{r} = \frac{\sum r \cdot n}{\sum n}, \tag{3.20}$$

where r is the distance from the center of the grid cell, and n is the number of particles at each grid cell. The parameters for this comparison were fairly basic. The temperature was 1 degree kelvin, there was no external current, the system size was 100x100, and there was only one particle. Multiple particle comparisons have been done, but because the jump probabilities are different depending on wether the site is empty or full, the comparison becomes much more complicated. The point of this benchmark was to make sure the complicated GPU Monte-Carlo integrator was working as expected. With 3 major components to this system, (calculating the energies, calculating the weights from the energies, and calculating a jump site from the weights), this was a simple way to make sure everything was working together

properly. Creating simple scripts to test more complicated scripts also became a useful tool in other parts of the research. For example, studying the behavior of the energy as a function of distance can be done via the Dias simulator, and outputs can be output for testing. But this can be complicated and the program may need to be changed and re-compiled in between tests. By writing a simple function in Octave and tuning the same parameters, the interaction between different energy sources could be observed more closely.

3.7.3 Fitting and Prediction

Other results also followed the expected trends. In Fig. 3.7 , One can see that as the temperature rises, the system slowly kills any aditional help from the E_{ij} component and it asymptotes to the jump distance related to the locality of the electron. In Fig. 3.8 , The dependance of current on voltage is almost exponential. In Fig. 3.10, one can see how the electrons can't go as far once the temperature is increased. A modified version of the simulator was run to explore the physics of electron transport as the system becomes saturated. The number of electrons in the system was slowly increased and simulations were run at different numbers of particles. In [17] they give approximate jump distances at various temperatures. We duplicated these and found similar values for $\bar{\mu} = .01$ and $\delta xy = .45$.

To conclude, we have designed and implemented a conserved order parameter Markov Chain Monte Carlo continuous time algorithm. We benchmarked it and found it to have the correct relations between temperature, average jump distance, current, and voltage. We then used it to predict seebeck effects for different combinations of dielectric constants.

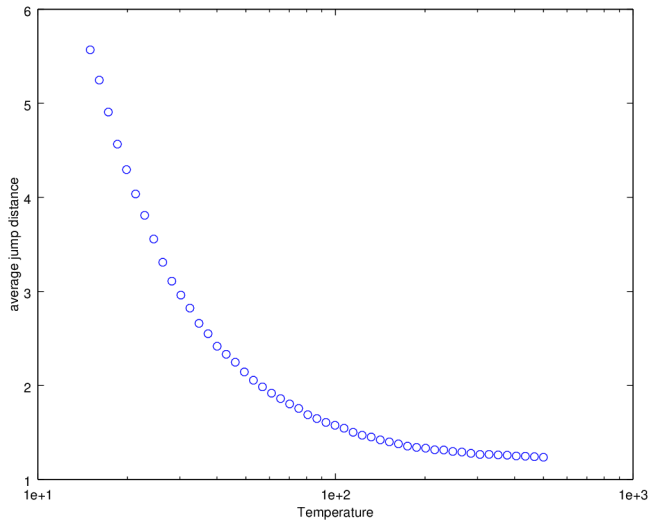

Figure 3.7: Temperature vs average jump distance .

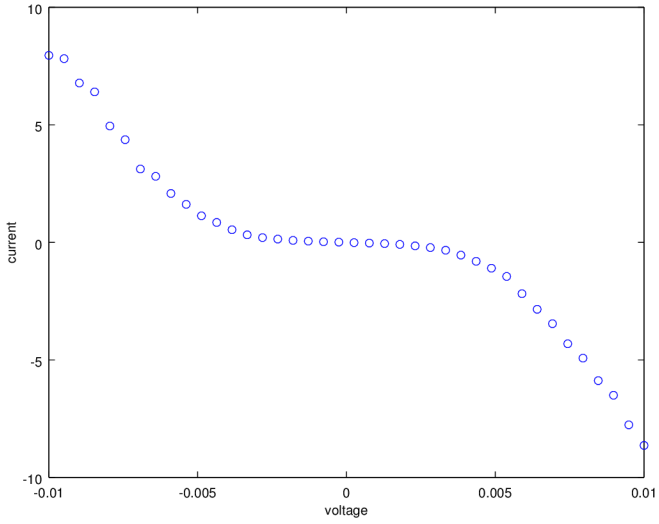

Figure 3.8: Current vs Voltage .

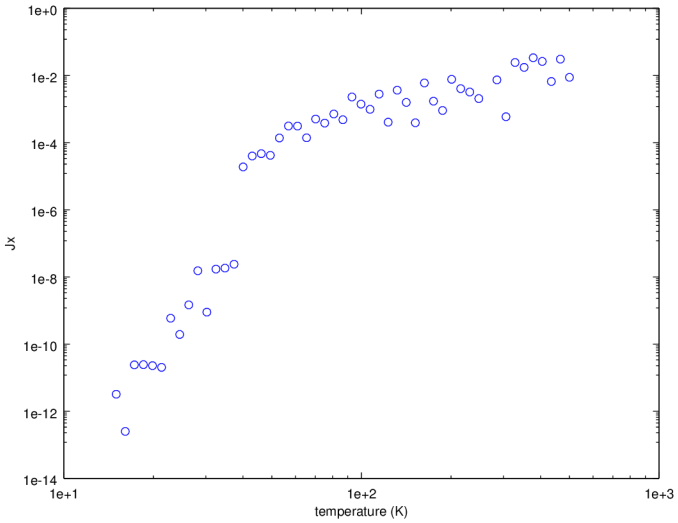

Figure 3.9: Temperature vs current .

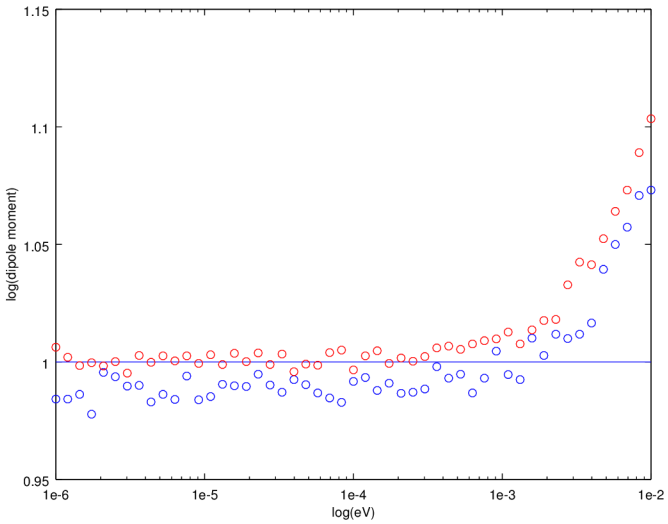

Figure 3.10: This is a plot of the voltage vs the dipole moment of the electrons. The red dots are for a system without a temperature gradient. The blue dots are for a system with a temperature gradient. When the dipole moment becomes 0, the thermal force is pushing with as much strength aas the electric force. Using the Seebeck equation, we can estimate the Seebeck coefficient to be 10μ

REFERENCES

[1] Mott, N. F.; Peierls, R. (1937). "Discussion of the paper by de Boer and Verwey". Proceedings of the Physical Society 49 (4S): 72

[2] A L Efros and B I Shklovskii , J. Phys. C8, L49 (1975)

[3] L.I. Glazman, M. Pustilnik, in "Nanophysics: Coherence and Transport," eds. H. Bouchiat et al. (Elsevier, 2005), pp. 427-478

[4] M. Kirkengen , J. Bergli, "Slow relaxation and equilibrium dynamics in a two-dimensional Coulomb glass: Demonstration of stretched exponential energy correlations" PHYSICAL REVIEW B 79, 075205 2009

[5] A. Aharony, Y. Zhang, M.P. Sarachik, "Universal Crossover in Variable Range Hopping with Coulomb Interactions", Physical Review Letters 1992

[6] D. Joungand, S. Khondaker, "Efros-Shklovskii variable range hopping in reduced graphene oxide sheets of varying carbon sp2 fraction", http://arxiv.org/pdf/1210.1876.pdf

[7] A. Glatz, I. Beloborodov, "Thermoelectric and Seebeck coefficients of granular metals", PHYSICAL REVIEW B 79, 235403 2009

[8] L. Chen, S. Gao, X. Zeng, A. Mehdizadeh Dehkordi,T. M. Tritt,and S. J. Poon, "Uncovering High Thermoelectric Figure of Merit in (Hf,Zr)NiSn Half-Heusler Alloys" , http://arxiv.org/pdf/1505.07773.pdf

[9] M. Ortuno , A. Somoza, "Coulomb Glasses", http://www.lancaster.ac.uk/users/esqn/windsor04/docs/cg.pdf

[10] I. S. Beloborodov, A. V. Lopatin, F. W. J. Hekking, R. Fazio, and V. M. Vinokur , "Thermal transport in granular metals ",Europhys. Lett. 69, 435 (2005)

[11] A. Glatz ,I. S. Beloborodov , "Nanogranular Thermoelectrics" , http://arxiv.org/pdf/0810.5545.pdf

[12] B. Gebhard, "The Mott Metal-Insulator Transition: Models and Methods", Springer 2003

[13] L. Glazman, M. Pustilnik, "Low-Temperature Transport Through A Quantum Dot", http://arxiv.org/pdf/cond-mat/0501007v2.pdf

[14] H. Liu, A. Pourret, P. Guyot-Sionnest, "Mott and Efros-Shklovskii Variable Range Hopping in CdSe Quantum Dots Films", ACS Nano, 2010, 4 (9), pp 5211-5216

[15] A. Glatz, V. Vinokur, J. Bergli, M. Kirkengen, Y. Galperin, "The Coulomb gap and low energy statistics for Coulomb glasses", Journal of Statistical Mechanics: Theory and Experiment, 2008

[16] C. Kittel, "Introduction to Solid State Physics", Wiley, 1996

[17] I. Beloborodov, A. Lopatin, V. Vinokur, K. Efetov, "Granular Electronic Systems", Reviews of Modern Physics, Volume 79, April-June 2007

[18] I. Sadovskyy, A. Koshelev, C. Phillips, D. Karpeev, A. Glatz, "Stable large-scale solver for Ginzburg-Landau equations for superconductors", Journal of Computational Physics, 09/2014

[19] E. Ferrero, A. Kolton, M. Palassini, "Parallel kinetic Monte Carlo simulation of Coulomb glasses" ,arXiv:1407.5026

[20] W. Krauth, "Statistical Mechanics: Algorithms and Computations", Oxford University Press, Oxford, 2006, pp. 3334

[21] M. Newman, G. Barkema, "Monte Carlo Methods in Statistical Physics", Oxford University Press, Oxford, 1999, pp. 41-42

[22] T. Sparks, M. Gaultois, A. Oliynyk, J. Brgoch, B. Meredig, "Data mining our way to the next generation of thermoelectrics", Scripta Materialia, Volume 111, 15 January 2016, Pages 1015

[23] R. Chandra, "Mechanical vapour compression refrigeration", Refrigeration and Air Conditioning, New Delhi, India: PHI Learning. p. 3. ISBN 81-203-3915-0.

[24] J. Brown, "Thermodynamics of a Rubber Band", American Journal of Physics, 31 (5): 397397, May 1963, doi:10.1119/1.1969535

[25] M. Miszczak, "GINZBURG-LANDAU SIMULATIONS OF NARROW SUPERCONDUCTING STRIPS" , Northern Illinois University, Department of Physics, 2015

[26] C. Kittel, "Introduction to Solid State Physics", 7th Ed., Wiley, (1996)

[27] O. Reichhardt, C. Reichhardt, "Commensurability, Jamming, and dynamics for vortices in funnel geometries" ,Physical Review B 81, 2010

[28] L. Haag, G. Zechner, W. Lang, M. Dosmailov, M. Bodea, J. Pedarnig "Strong vortex matching effects in YBCO films with periodic modulations of the superconducting order parameter fabricated by masked ion irradiation", Physica C: Superconductivity, Volume 503, 2014, pg 75-81

[29] S. Horii, M. Haruta, A. Ichinose, T. Doi, "Evidence for enhancement of vortex matching field above 5 T and oxygen-deficient annuli around barium-niobate nanorods", Journal of Applied Physics 118, 133907 (2015)

[30] F.Rizzo, A.Augieri, A. Armenio, V. Galluzzi, A. Mancini, V. Pinto, A. Rufoloni, A. Vannozzi, M. Bianchetti, A. Kursumovic, J. MacManus-Driscoll, A. Meledin, G. Van Tendeloo, G. Celentano, "Enhanced 77 K vortex-pinning in Y Ba2Cu3O7x films with Ba2Y TaO6 and mixed Ba2Y TaO6 + Ba2Y NbO6 nano-columnar inclusions with irreversibility field to 11 T", APL Mater. 4, 061101 (2016); doi: 10.1063/1.4953436

[31] A. Thakur, S. Ooi, S. Chockalingam, J. Jesudasan, P. Raychaudhuri, K. Hirata, "Vortex matching effect in engineered thin films of NbN", APPLIED PHYSICS LETTERS 94, 262501 2009

[32] P. Sabatino, C. Cirillo, G. Carapella, M. Trezza, and C. Attanasio, "High field vortex matching effects in superconducting Nb thin films with a nanometersized square array of antidots", Journal of Applied Physics 108, 053906 (2010)

[33] Q. Lu, O. Reichhardt, C. Reichhardt, "Reversible vortex ratchet effects and ordering in superconductors with simple asymmetric potential arrays", PHYSICAL REVIEW B 75, 2007

[34] J. Wambaugh, C. Reichhardt, C. Olson, F. Marchesoni , F. Nori, "Superconducting fluxon pumps and lenses", VOLUME 83, NUMBER 24 PHYSICAL REVIEW LETTERS, 1999

[35] K. Yu, M. Hesselberth, P. Kes, B. Plourde, "Vortex dynamics in superconducting channels with periodic constrictions", PHYSICAL REVIEW B 81, 2010

[36] G. Berdiyorov, M. Miloevi, F. Peeters, "Vortex configurations and critical parameters in superconducting thin films containing antidot arrays: Nonlinear Ginzburg-Landau theory", PHYSICAL REVIEW B 74, 2006

[37] N. Mott, "Conduction in glasses containing transition metal ions", Cambridge, Journal of non-crystaline solids, 1968

[38] L. Glazman, M. Pustilnik,"LOW-TEMPERATURE TRANSPORT THROUGH A QUANTUM DOT" arXiv:cond-mat/0501007 v2 10 Oct 2005

[39] D. Tsigankov, A. Efros, "Variable Range Hopping in Two-Dimensional Systems of Interacting Electrons", VOLUME 88, NUMBER 17 PHYSICAL REVIEW LETTERS 2002

[40] W. Young and E. Elcock,"Monte Carlo studies of vacancy migration in binary ordered alloys", Proceedings of the Physical Society 89 (1966) 735.

[41] S. Serebrinsky, "Physical time scale in kinetic Monte Carlo simulations of continuous-time Markov chains", PHYSICAL REVIEW E 83, (2011)

[42] B. Abeles, P. Sheng, M. Coutts, Y. Arie, "Structural and electrical properties of granular metal films", Advances in Physics, 1975

[43] D. Hubbard, D. Samuelson, "Modeling Without Measurements". OR/MS: 2833. 2009

[44] M. Kalos, P. Whitlock, "Monte Carlo Methods", Wiley-Blackwell, 2008

[45] B. Everitt, "The Cambridge Dictionary of Statistics", CUP. ISBN 0-521-81099-X, 2002

[46] L. van Dommelen, "A.11 Thermoelectric effects". Eng.fsu.edu. 2002-02-01. Retrieved 2013-04-22.

[47] W. Kwok, U. Welp, A. Glatz1, A. Koshelev1, K. Kihlstrom1, G. Crabtree, "Vortices in high-performance high-temperature superconductors", Reports on Progress in Physics, 2016

[48] D. Rowe, "Thermoelectrics Handbook: Macro to Nano.", CRC Press. ISBN 978-1-4200-3890-3., 2005